UNIVERSITY OF CALIFORNIA, BERKELEY

BERKELEY • DAVIS • IRVINE • LOS ANGELES • RIVERSIDE • SAN DIEGO • SAN FRANCISCO

SANTA BARBARA • SANTA CRUZ

SEISMOGRAPHIC STATION
DEPARTMENT OF GEOLOGY AND GEOPHYSICS

BERKELEY, CALIFORNIA 9472

01 March 1976

Director, ARPA
1400 Wilson Boulevard
Arlington, Virginia 22209

Attn: Program Management

Semi-Annual
TECHNICAL REPORT NO. 5, 01 July — 31 December 1975

ARPA Order No. 1827
Program Code 3F10
Grantee: The Regents of the University of California
Effective Date of Grant: 01 June 1973
Grant Termination Date: 30 Sept 1976
Amount of Grant: $215,068
Grant No.: AFOSR-73-2563 ARPA Order-1827
Principal Investigators:

T. V. McEvilly	L. R. Johnson
(415) 642-4494	(415) 642-1275

Short Title of Work: BROADBAND DISCRIMINATION STUDIES

T. V. McEvilly

L. R. Johnson

Sponsored by
Advanced Research Projects Agency
ARPA Order No. 1827

SECURITY CLASSIFICATION OF THIS PAGE (When Data Entered)

REPORT DOCUMENTATION PAGE

READ INSTRUCTIONS BEFORE COMPLETING FORM

1. REPORT NUMBER	2. GOVT ACCESSION NO. AD-A101 743
3. RECIPIENT'S CATALOG NUMBER	
4. TITLE (and Subtitle) BROADBAND DISCRIMINATION STUDIES	5. TYPE OF REPORT & PERIOD COVERED Semi-annual Technical 01 July - 31 Dec 1975
	6. PERFORMING ORG. REPORT NUMBER
7. AUTHOR(s) T. V. McEvilly L. R. Johnson	8. CONTRACT OR GRANT NUMBER(s) FOSR-73-2563A
9. PERFORMING ORGANIZATION NAME AND ADDRESS Seismographic Station University of California Berkeley, CA 94720	10. PROGRAM ELEMENT, PROJECT, TASK AREA & WORK UNIT NUMBERS 62701E ARPA Order No. 1827
11. CONTROLLING OFFICE NAME AND ADDRESS ARPA/NMR 1400 Wilson Blvd. Arlington, VA 22209	12. REPORT DATE 01 March 1976
	13. NUMBER OF PAGES 48
14. MONITORING AGENCY NAME & ADDRESS (if different from Controlling Office) AFOSR/NP 1400 Wilson Blvd. Arlington, VA 22209	15. SECURITY CLASS. (of this report) Unclassified
	15a. DECLASSIFICATION/DOWNGRADING SCHEDULE

16. DISTRIBUTION STATEMENT (of this Report)

Approved for public release; distribution unlimited

17. DISTRIBUTION STATEMENT (of the abstract entered in Block 20, if different from Report)

18. SUPPLEMENTARY NOTES

19. KEY WORDS (Continue on reverse side if necessary and identify by block number)

seismology
seismometry
earthquake source
explosion source
anelasticity
attenuation

20. ABSTRACT (Continue on reverse side if necessary and identify by block number)

Broadband data are accumulating in the Berkeley system and provide excellent data on teleseisms and local earthquakes and explosions. The August 1975 Oroville earthquake provided a successful test of the broadband system under relatively strong (1-2 mm ground displacement) ground displacement. Attenuation studies continue with extension of variational formulation to dissipative surface wave propagation and observations of local/regional earthquakes over a broad spectral band.

DD FORM 1 JAN 73 1473 EDITION OF 1 NOV 65 IS OBSOLETE

SECURITY CLASSIFICATION OF THIS PAGE (When Data Entered)

TABLE OF CONTENTS

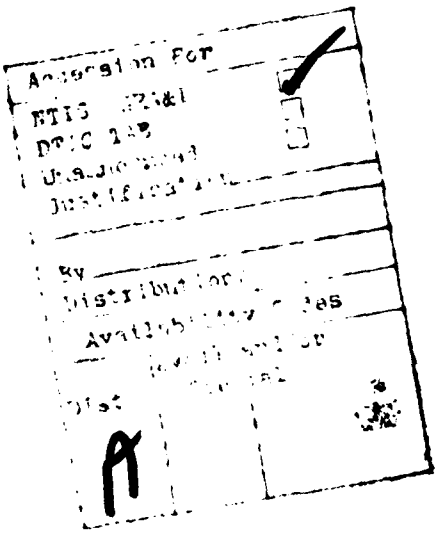

REPORT SUMMARY

Broadband data are accumulating on Berkeley network stations for earthquakes and explosions. The variational formulation for elastic surface waves has been extended to the case of dissipative media. Broadband spectral data on Sierra Nevada earthquakes appear to be unaffected by Q, yielding data crucial to discrimination among various earthquake source models. The Oroville earthquakes of August 1975 have been investigated. The main shock produced ground displacements of 1-2 mm at Jamestown (JAS) and Whiskeytown (WDC) broadband stations, providing a test of system performance under relatively strong motion. Both systems behaved well, producing excellent records of the strong motion with no indications of spurious responses commonly seen in long period systems.

A VARIATIONAL FORMULATION FOR LOVE WAVES IN A LAYERED ANELASTIC SOLID *

Walt Silva

Department of Geology and Geophysics
University of California
Berkeley, California

ABSTRACT

A method is presented which allows the variational formulation for elastic surface waves to be extended to the case of dissipative media. With this formulation, correct to second order in the loss, Rayleigh's principle can be applied to perturbations of the Rayleigh quotient to yield group velocity without numerical differentiation. Other perturbations can be used to find the change in phase or group velocity due to changes in loss, density, or moduli.

* In press, Geoph. J. R. A. S., 1976.

INTRODUCTION

The use of Rayleigh's principle is of considerable importance in surface wave calculations. As suggested by Meissner (1926) and Jeffreys (1959, 1961) and amended by Harkrider (1968) it has replaced numerical methods with an exact formulation for calculating group velocities. In addition, Rayleigh's principle may be used to calculate the effect on the velocity dispersion due to small perturbations in the elastic parameters. This type of information is, of course, most essential in solving inverse problems.

However, in its usual form, Rayleigh's principle is inadequate for dissipative systems since its use requires equating the time average kinetic and potential energies. This result follows from the virial theorem and imposes a vanishing Lagrangian for the system.

The purpose of the following development is to construct a Lagrangian for a non-conservative system which vanishes and then apply Rayleigh's principle to the resulting equation. This can be done by writing a Lagrangian for two systems operating simultaneously with one losing energy as the other gains energy, so that the total energy is conserved. An estimate of the error introduced in combining the systems is given in the appendix.

The development will be for Love waves in order to simplify the equations. The extension to Rayleigh waves follows naturally.

FORMULATION

As a working example, we shall consider Love waves propagated along the surface of a vertically heterogenous (layered) attenuating half-space. The usual equation to be satisfied in each layer is

$$\mu_R \nabla^2 u + \frac{\mu_I}{\omega} \nabla^2 \dot{u} = \rho \ddot{u} \qquad (1)$$

where u is the transverse particle displacement, ρ is the medium density, and μ_R and μ_I are the conservative and non-conservative Lamé parameters, respectively, which are in general frequency dependent (Borcherdt 1971, Silva 1975). We take as the solution to equation (1)

$$u = V(z)\, e^{-A_x x} \cos(P_x x - \omega t) \qquad (2)$$

where P_x is the spatial frequency such that the horizontal anelastic phase velocity c is given by $c = \frac{\omega}{P_x}$ and A_x is the horizontal attenuation factor. Application of the usual boundary conditions results in the continuity of both P_x and A_x. They then represent eigenvalues to be determined for propagating modes. The attenuation factor may be defined as

$$A_x = \frac{\omega}{c}\left[\frac{-1 + \sqrt{1 + Q_L^{-2}}}{1 + \sqrt{1 + Q_L^{-2}}}\right]^{\frac{1}{2}} \approx \frac{\omega}{2 c Q_L} \qquad (3)$$

where Q_L represents the effective quality factor for the spatial decay of the surface wave. Equation (3) can then be interpreted as the projection of the attenuation in the propagation direction. The

shear quality factor Q_s is defined as

$$Q_s^{-1} = \frac{1}{2\pi} \frac{\Delta E}{E} = \frac{\mu_I}{\mu_R} \tag{4}$$

where ΔE is the energy lost and E the peak energy stored, both per cycle.

At this point we introduce the mirror image system which is taken to exist simultaneously with the original field. Since this field gains energy exactly as the first loses energy, we can write the field equation as

$$\mu_R \nabla^2 u^+ - \frac{\mu_I}{\omega} \nabla^2 \dot{u}^+ = \rho \ddot{u}^+ \tag{5}$$

with the corresponding solution,

$$u = V(z) e^{A_x x} \cos(P_x x - \omega t) \tag{6}$$

It is seen then that the only difference in the systems is in the sign of μ_I. This then affects only the sign of the attenuation constant and yields the same spatial frequencies as equation (2).

In order to construct a conservative Lagrangian density we make use of the following form (Morse and Feshbach, 1953; Moisewitsch, 1966).

$$\mathcal{L} = \rho \dot{u} \dot{u}^+ - \frac{1}{2} \frac{\mu_I}{\omega} \nabla^2 \left[u \dot{u}^+ - \dot{u} u^+ \right] - \mu_R \left[\frac{\partial u}{\partial x} \frac{\partial u^+}{\partial x} + \frac{\partial u}{\partial z} \frac{\partial u^+}{\partial z} \right] \tag{7}$$

This yields an invariant Lagrangian, since u^+ increases in amplitude exactly as u decreases.

The corresponding Euler-Lagrange equations become:

$$\frac{\partial \mathcal{L}}{\partial u} - \frac{d}{dt}\frac{\partial \mathcal{L}}{\partial \dot{u}} - \frac{d}{dx}\frac{\partial \mathcal{L}}{\partial u_x} - \frac{d}{dz}\frac{\partial \mathcal{L}}{\partial u_z} = 0 \qquad (8)$$

$$\frac{\partial \mathcal{L}}{\partial u^+} - \frac{d}{dt}\frac{\partial \mathcal{L}}{\partial \dot{u}^+} - \frac{d}{dx}\frac{\partial \mathcal{L}}{\partial u_x^+} - \frac{d}{dz}\frac{\partial \mathcal{L}}{\partial u_z^+} = 0$$

Direct substitution of equation (7) into equation (8) yields equations (1) and (5). We now substitute the solutions (equations (2) and (5)) into equation (7) and then space-time integrate the Lagrangian density to yield the Lagrangian of the combined system. In the time and x integrations, where periodic solutions were assumed, the integrations result simply in averages.

Defining L as the Lagrangian of the combined system, we can write:

$$L = \omega^2 \int \rho V V^+ \, dz - \left(P_x^2 - A_x^2\right) \int \mu_R V V^+ \, dz - \int \mu_I V' V^{+\prime} \, dz \qquad (9)$$

The first term is interpreted as a time average kinetic energy and the remaining two terms as a time average potential energy. This allows the application of the virial theorem (Moisewitsch, 1966) which states that for a conservative system which is quadratic in its potential energy the time average potential and kinetic energies are equal.

We may then put equation (9) into the form of the Rayleigh quotient:

$$\omega^2 I_0 = \left(P_x^2 - A_x^2 \right) I_1 + I_2 \qquad (10)$$

with the energy integrals

$$I_0 = \int \rho V V^+ dz \quad ; \quad I_1 = \int \mu_R V V^+ dz \; ;$$

$$I_2 = \int \mu_R V' V^{+\prime} dz$$

Application of Rayleigh's Principle

Rayleigh's principle states that for a given Rayleigh quotient, as in equation (10), any eigenvectors, correct to first order, will yield the eigenvalue appropriate to that mode correct to second order. This can be stated more precisely by considering the perturbation to equation (10) due to a small change in v and v^+.

$$\omega^2 \delta I_0 = \left(P_x^2 - A_x^2 \right) \delta I_1 + \delta I_2 \qquad (11)$$

where the perturbed energy integrals are given by:

$$\delta I_0 = \int \rho \, \delta (V V^+) dz \quad ; \quad \delta I_1 = \int \mu_R \, \delta (V V^+) dz \; ;$$

$$\delta I_2 = \int \mu_R \, \delta (V' V^{+\prime}) dz$$

Making use of equation (11) the new eigenvalues correct to second order may be calculated.

$$(\omega + \delta\omega)\left[I_0 + \delta I_0\right] = \left[(P_x + \delta P_x)^2 - (A_x + \delta A_x)^2\right] \cdot \left[I_1 + \delta I_1\right] + \left[I_2 + \delta I_2\right] \qquad (12)$$

Using equations (10) and (11) and neglecting second order in small quantities equation (12) becomes:

$$\omega\, \delta\omega\, I_0 = \left(P_x\, \delta P_x - A_x\, \delta A_x\right) I_1 \qquad (13)$$

and using $c = \frac{\omega}{P_x}$ for phase velocity, $U = \frac{\delta\omega}{\delta P_x}$ for group velocity, we can rewrite equation (13) in the following form:

$$U = \left[1 - \frac{A_x\, \delta A_x}{P_x\, \delta P_x}\right] \frac{I_1}{c\, I_0} \qquad (14)$$

At this point Rayleigh's principle may again be invoked and the elastic eigenvectors may be used in the calculation of the energy integrals.

In order to estimate the perturbation in $A_x(\delta A_x)$ due to a frequency perturbation, we use equation (3) and neglect the term containing $\frac{\delta Q_L}{\delta\omega}$. This is correct to at least second order in Q_L^{-1} since Q_L is a slowly varying function of frequency and the term has a coefficient of Q_L^{-2}. (It can, in fact, be estimated using a difference scheme since $Q_L(\omega)$ is known from the eigenvalues.)

With this approximation equation (14) becomes

$$U = \left[\frac{2}{1 + \sqrt{1 + Q_L^{-2}}}\right] \frac{I_1}{c\, I_0} \qquad (15)$$

which reduces to the usual elastic expression as $Q_L \to \infty$ and $v^+ \to v$. This expression, which is an approximation correct to at least second order in the loss, is thought to be preferable to numerical differentiation of the phase dispersion curve.

In order to calculate the effect on Q_L due to a small change in Q_S we must first find an expression for μ_R in terms of v_S and Q_S. This can be done by assuming a solution of equation (1) of the form

$$u = u_o e^{-i(\underset{\sim}{K}\cdot\underset{\sim}{X} - \omega t)} \tag{16}$$

where $\underset{\sim}{K} = \underset{\sim}{P} - i\,\underset{\sim}{A}$ (Borcherdt, 1973). Substituting this into equation (1), and defining the shear velocity v_S as that of homogeneous waves ($\underset{\sim}{P}$ parallel to $\underset{\sim}{A}$) we can write:

$$\mu_R = \rho \frac{V_S^2}{2}\left[\frac{1 + \sqrt{1 + Q_S^{-2}}}{1 + Q_S^{-2}}\right] \tag{17}$$

By substituting equation (17) into I_1 and I_2 we are able to explicitly calculate the change in the Love wave quality factor δQ_L due to a change δQ_S in the energy integrals. We can write the entire perturbed Rayleigh quotient at constant frequency as:

$$\omega^2\left[I_o + \delta I_o\right] = \left[(P_x + \delta P_x)^2 - (A_x + \delta A_x)^2\right] \cdot \tag{18}$$

$$\left[I_1 + \delta I_1 + \delta_{Q_S} I_1\right] + \left[I_2 + \delta I_2 + \delta_{Q_S} I_2\right]$$

where we have defined

$$\delta_{Q_S} I_1 = \int \rho \frac{V_S^2}{2} V V^* \delta\left[\frac{1 + \sqrt{1 + Q_S^{-2}}}{1 + Q_S^{-2}}\right] dz$$

$$\tag{19}$$

$$\delta_{Q_S} I_2 = \int \rho \frac{V_S^2}{2} V' V^{*\prime} \delta\left[\frac{1 + \sqrt{1 + Q_S^{-2}}}{1 + Q_S^{-2}}\right] dz$$

Using equations (3), (10) and (11) and neglecting second order terms in small quantities we can reduce equation (18) to:

$$0 = 2\left[P_x \delta P_x - A_x \delta A_x\right] I_1 + \left[P_x^2 - A_x^2\right] \delta_{Q_S} I_1 + \delta_{Q_S} I_2 \tag{20}$$

Writing equation (3) as

$$A_x = P_x f(Q_L) \; ; \; f(Q_L) = \left[\frac{-1 + \sqrt{1 + Q_L^{-2}}}{1 + \sqrt{1 + Q_L^{-2}}}\right]^{\frac{1}{2}} \tag{21}$$

we can express the perturbation in A_X due to a change in Q_L:

$$\delta A_x = \delta P_x f(Q_L) + P_x \delta f(Q_L) \tag{22}$$

Neglecting the first term since it is at least second order in the loss we then have from equation (20);

$$\delta f(Q_L) = \frac{\delta A_x}{P_x} = \frac{1}{2 P_x A_x I_1}\left[\left(P_x^2 - A_x^2\right) \delta_{Q_S} I_1 + \delta_{Q_S} I_2\right] \tag{23}$$

and to the same order we have from equation (3)

$$\delta Q_L \approx -2 Q_L^2 \delta f(Q_L) \tag{24}$$

This formulation then allows estimates to be made on the change in the Love wave quality factor or attenuation factor due to a small change in the shear quality factor. Further perturbations involving v_s and ρ can be made along similar lines (Harkrider, 1968).

The extension to Rayleigh waves will, of course, be more tedious since equation (9) will now contain four integrals. In addition, equation (18) now must consider Q_p as well as Q_s. The situation is unpleasant though tractable and the group velocity is presently being programmed by the author.

APPENDIX

In order to estimate the error introduced by the formulation in this paper, presented /we shall consider a plane shear wave propagating along the x direction in a Voigt solid (Kolsky, 1963).

The equation of motion can be written

$$\mu \frac{\partial^2 w}{\partial x^2} + \mu' \frac{\partial^2 \dot{w}}{\partial x^2} = \rho \ddot{w} \qquad (1)$$

with the solution.

$$w = e^{-Ax} \cos(\omega t - Px) \qquad (2)$$

We may define the quality factor for this system as:

$$Q^{-1} = \frac{\mu' \omega}{\mu} \qquad (3)$$

Substituting equations (3) and (2) into (1) we arrive at:

$$P^2 - A^2 = \frac{\omega^2 \rho}{\mu \left(1 + Q^{-2}\right)} \qquad (4)$$

On the other hand, if we had applied the Lagrangian formulation pre- in this paper sented/the results would have been:

$$P^2 - A^2 = \omega^2 \frac{\rho}{\mu} \qquad (5)$$

which is correct to second order in the loss.

ACKNOWLEDGMENTS

I would like to thank Lane Johnson for many helpful comments. This research was supported by the Advanced Research Projects Agency of the Department of Defense and was monitored by the Air Force Office of Scientific Research under Grant No. AFOSR-73-2563.

REFERENCES

Borcherdt, R., Energy and plane waves in linear viscoelastic media, J. Geophys. Res., 73, 14, 2442-2453, 1973.

Borcherdt, R., Inhomogenous body and surface waves in a generalized viscoelastic half-space, Ph.D. thesis, 308 pp., Univ. of Calif., Berkeley, 1971.

Harkrider, D., The perturbation of Love wave spectra, B.S.S.A., 58, 3, 861-880, 1968.

Jeffreys, H., Small corrections in the theory of surface waves, Geophys. J. R. astro. Soc., 6, 1, 227-229, 1963.

Jeffreys, H., The Earth, 4th edition, Cambridge: University Press, 1959.

Kolsky, H., Stress Waves in Solids, Dover Pub., Inc., New York 1963.

Meissner, E., Proc. 2nd Congr. Appl. Math., Zürich, 3-11, 1926.

Moisewitsch, B. L., Variational Principles, p.20, Interscience Publishers, London 1966.

Morse, P. M., and H. Feshbach, Methods of Theoretical Physics, p. 298, McGraw-Hill, New York 1953.

Silva, W., Body waves in a layered anelastic solid, submitted to B.S.S.A., 1975.

P- AND SV-WAVE CORNER FREQUENCIES OVER LOW-LOSS PATHS: A DISCRIMINANT FOR EARTHQUAKE SOURCE THEORIES?*

William A. Peppin
Seismological Laboratory
University of Nevada
Reno, Nevada 89507

and

Gerald W. Simila
Seismographic Station
University of California
Berkeley, California 94720

ABSTRACT

Broadband data recorded at Jamestown, California, yield displacement spectrum corner frequencies for P- and SV-waves from 18 trans-Sierra Nevada events in the range $3.2 \leq M_L \leq 4.0$. The ratio R of P to SV corner frequency is .96 ± .17 Hz for these events, which sample a wide range of source azimuths and focal mechanisms. Assumptions of a flat far-field source spectrum and frequency-independent attenuation in the 1-20 Hz band lead to Q_β not less than 480. Many recent source theories predict factor-of-two or more variation of R with azimuth, and significant deviation of its average value from unity; such source models apparently do not apply to earthquakes studied here. Previous studies of R by Molnar et al. (1973), Stump (1974), and Bakun et al. (1975) reach different conclusions. We interpret this discrepancy not as a contradiction, but as an indication that R may be an extremely useful source-model discriminant, its variation indicating that different models may apply in different source regions. Well-determined measurements of R may lead to a clearer understanding of the physical processes associated with earthquakes.

* This is a shortened version of an article with the same title submitted to J. Phs. Earth, 1976.

INTRODUCTION

Recent papers on earthquake source theory differ quite markedly in their predictions of the frequency content of P and S waves leaving the source. High-quality data have been used by Molnar et al. (1973), Stump (1974) and Bakun et al. (1975) to investigate the frequency content of P- and S-waves, but with differing results. The present study addresses these discrepancies with analysis of the broadband vertical-component seismograph system at Jamestown (JAS), California. The system is described in previous Technical Reports for this Contract.

DATA

As JAS is situated in the Sierra Nevada batholith, it monitors low-loss granite travel paths for trans-Sierra Nevada earthquakes. All well-recorded trans Sierra Nevada events from 06 July 1974 to 31 August, 1975, and a representative sampling of the many Oroville earthquake aftershocks were analyzed. Epicenter and magnitude information is given in Table 1 Event nos. 1-18). The nature of the travel paths to JAS can be seen in Figure 1, which also shows the distribution of exposed granites. Representative seismograms subjected to analysis are shown in Figure 2.

PROCESSING

The JAS seismograms were digitized from FM magnetic tape at 25 or 50 samples per second after analog alias filtering. A 10% cosine taper was applied and spectral moduli were computed for the entire vertical Pg or Sg phase, then smoothed (3-point triangle window). The instrument response was removed, but not the 10-Hz alias filter response. Identical processing was applied to a noise sample (different for P than for SV) preceding each

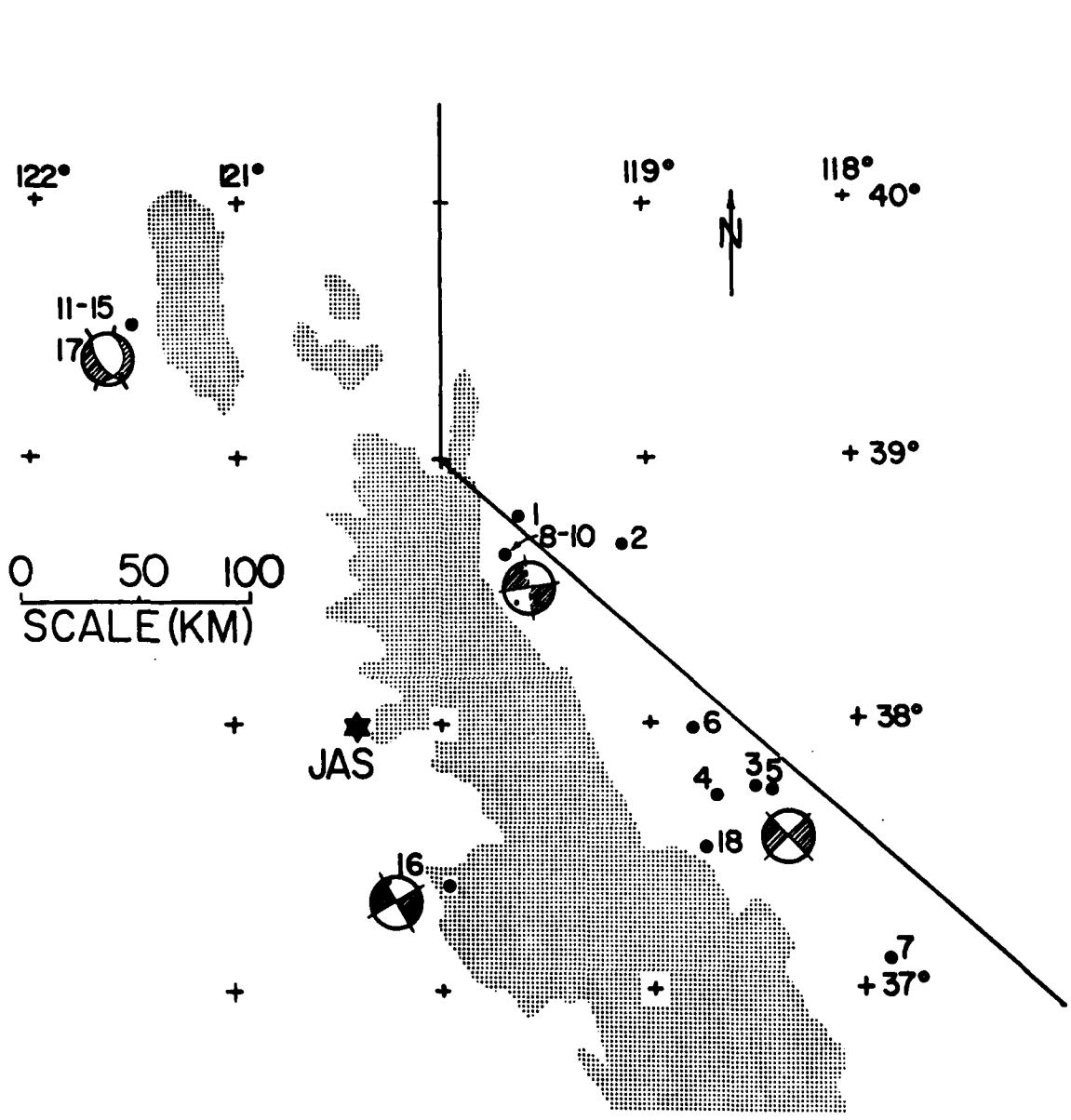

Figure 1 Location of the trans-Sierra Nevada events (black dots) relative to station JAS (black star). The numbers beside each dot are the event numbers in Table 1. The shaded areas are exposed granitic rocks associated with the Sierra Nevada batholith. Focal mechanisms representing the four source regions are presented; the small dots within each solution give the approximate Pg travel path to JAS.

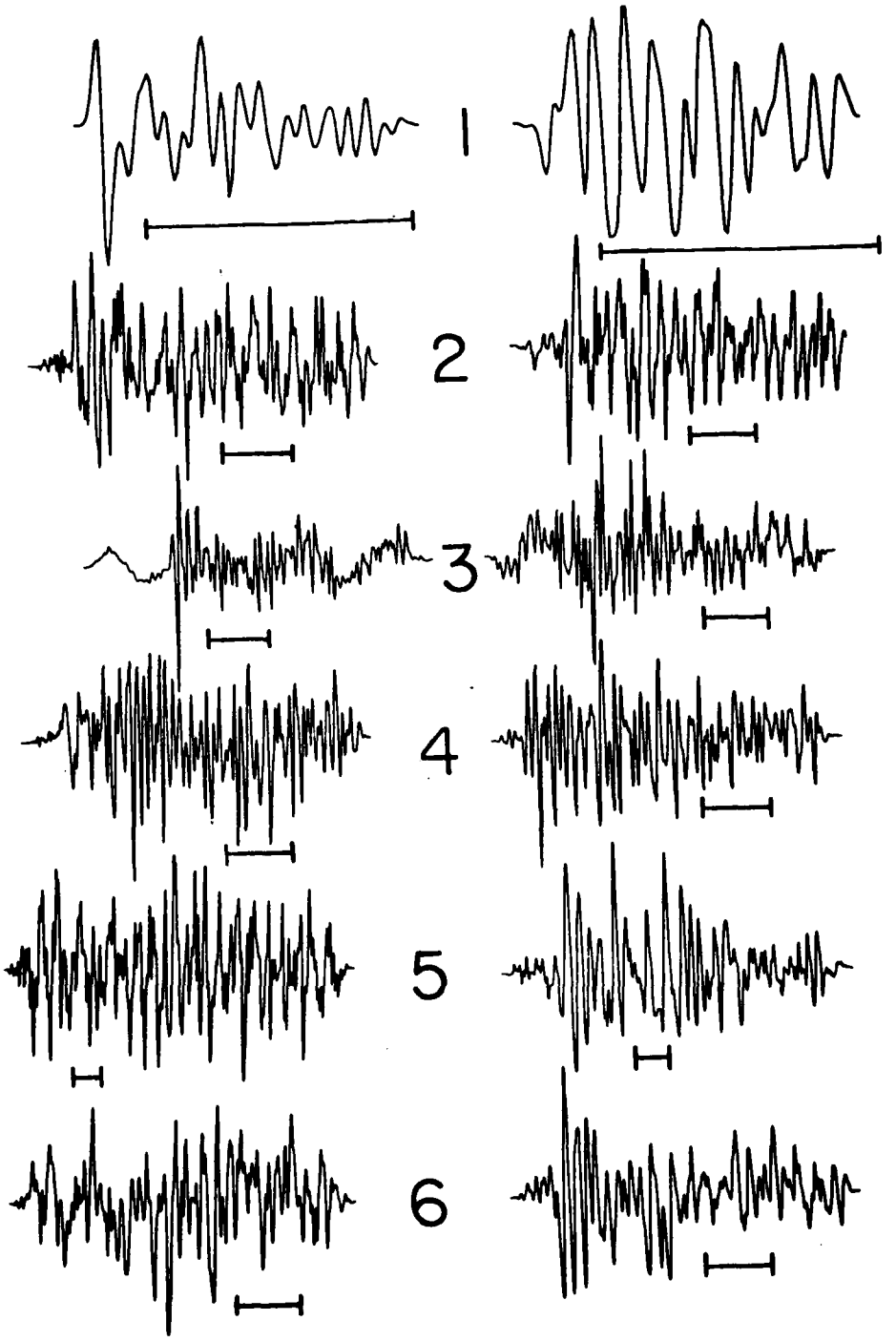

Figure 2. P (left) and SV (right) seismograms at JAS. The bracket beneath the trace is 2 sec long.

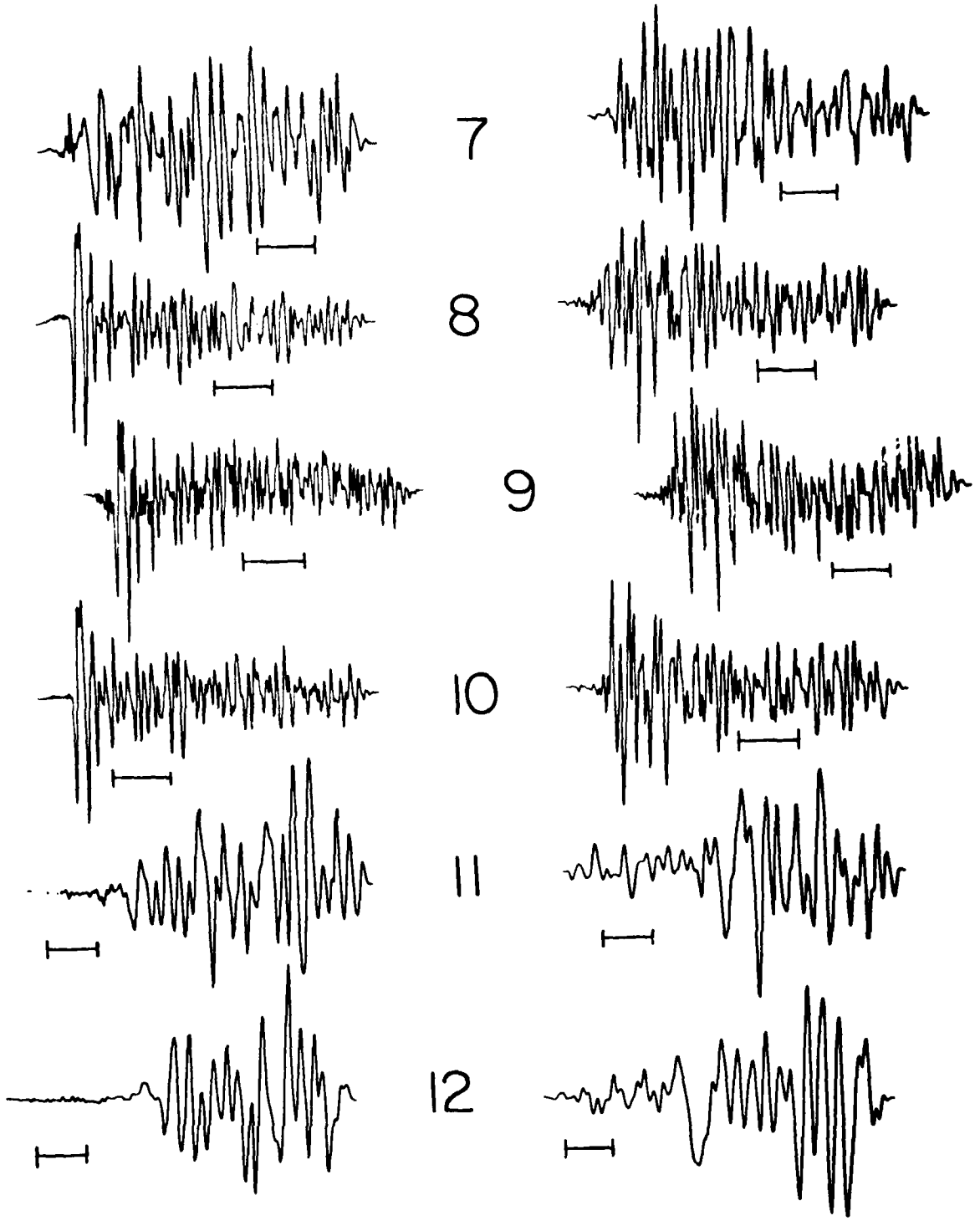

Figure 2 (cont).

event. Example spectra are shown in Figure 3. Corner frequencies for all spectra were estimated by overlaying the spectra with a template, flat at long period and decaying to high frequency as frequency squared or cubed (whichever fit the individual spectrum better). The black dots in Figure 3 show the corner frequencies selected. These are given together with an estimate of their uncertainty in Table 1.

RESULTS

The corner frequencies were used to compute R, and these values are given in Table 1. The observed value of R for all 18 earthquakes is .96 ± .17. The earthquakes represent at least four distinct source areas at widely varying azimuths from JAS; thus, we can safely say that these values, showing equal P- and S-wave corner frequencies to a precision of 20%, are representative of earthquakes in the Sierra Nevada province. The values of R are plotted in Figure 4 along with data from Molnar et al. (1973) and Bakun et al. (1975). The main point of this paper is that these three studies, each based on excellent data, give quite different and distinctive patterns for R in the three source regions represented.

DISCUSSION

Propagation Effects

We would hope the observed values of R reflect conditions at the source, but, since the travel paths are long (Table 1), distortion caused by propagation might be severe. We consider now two forms of this distortion: reverberations among crustal layers and anelastic attenuation, along with evidence suggesting neither effect alters observed frequencies appreciably, and thus our observations of R do indeed apply to the source characteristics of these earthquakes.

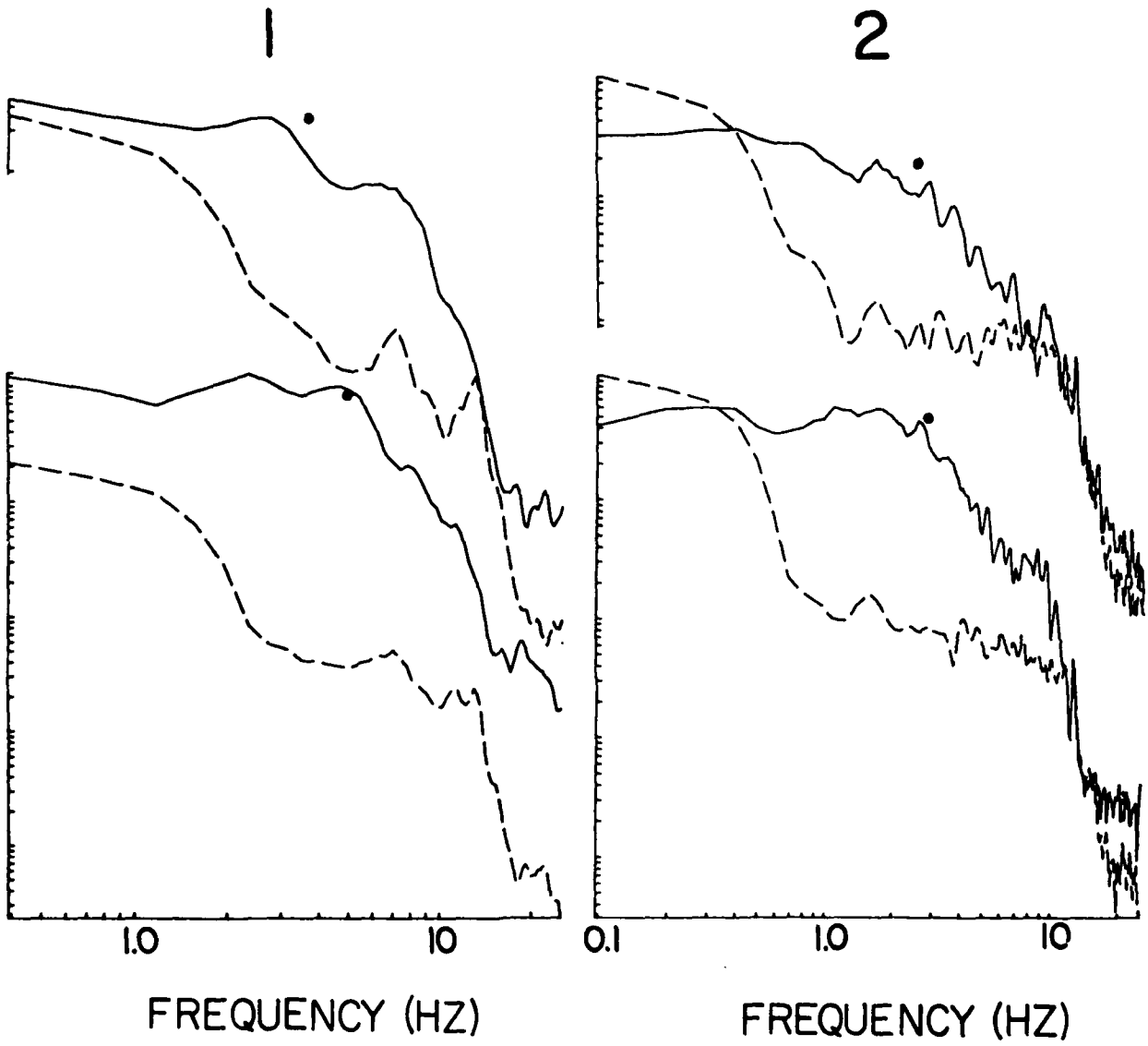

Figure 3. P (upper) and SV (lower) spectra for two events. Dashed lines are noise spectra, dots show corner frequencies picked.

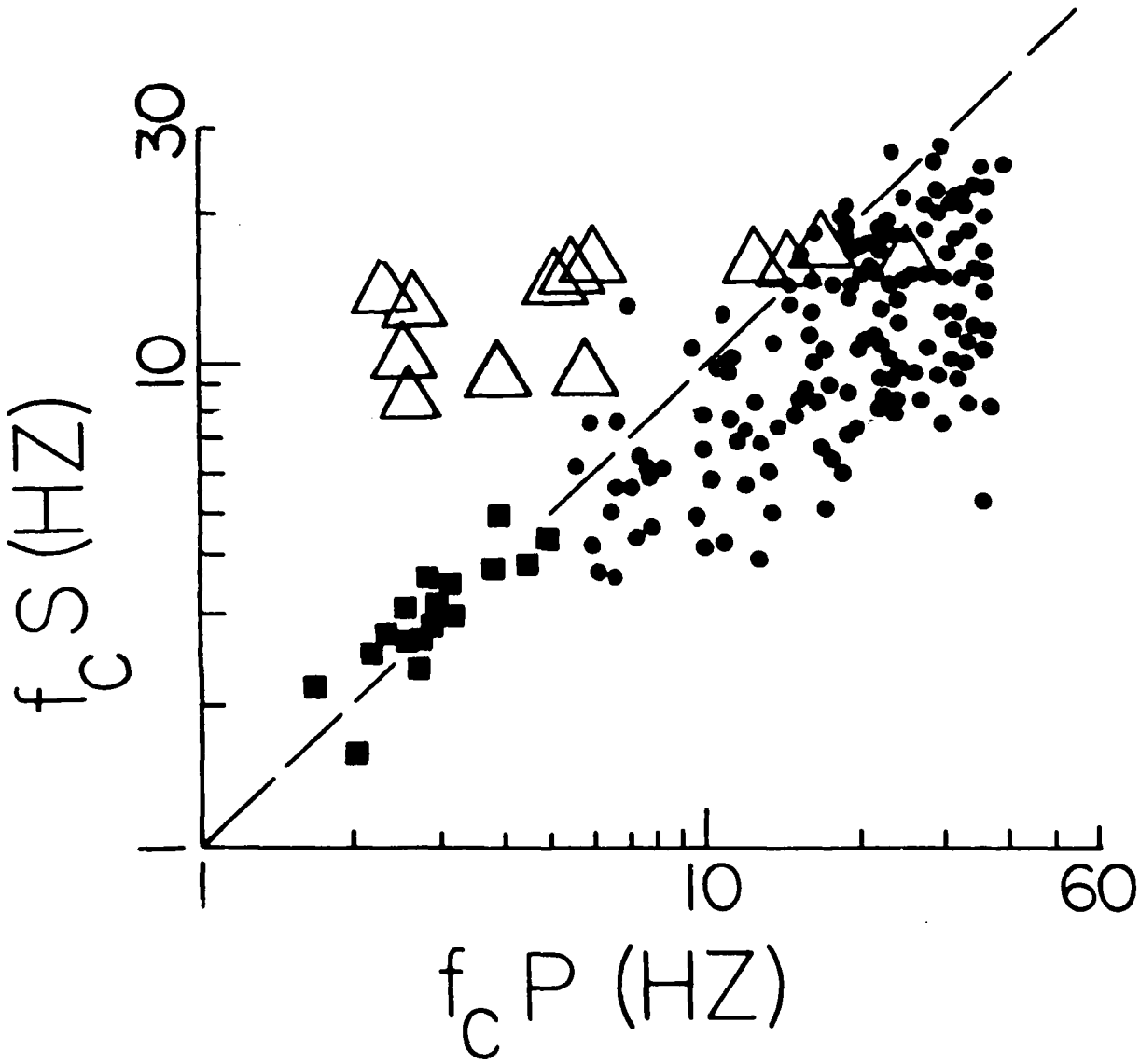

Figure 4: Summary of published data on corner frequencies of P- and S-waves. Small round dots are from Molnar et al. (1973); open triangles are from Bakun et al. (1975); solid black squares are from this study, Table 1.

Layer reverberation would appear to cause little distortion of the spectra because the travel paths - through crystalline rock - are quite homogeneous. This is illustrated by the very simple form of the P-phase for Events 3, 8, 9, and 10 in Figure 2.

Anelastic attenuation:

For frequency-independent attenuation in the 1-20 Hz band, we have spectral correction A(f) (Asada and Takano, 1963)

$$A(f) \propto \exp\{ -\pi f t/Q\} \qquad (1)$$

If the spectral corner frequency f_c is defined as that frequency at which the observed spectrum is 6 db below the (assumed flat) long-period spectral component, we can estimate Q from (1) as

$$Q \simeq -\pi f_c t/\ln(.5) = 4.5\ f_c t \qquad (2)$$

provided that Q is responsible for the corner frequency. Therefore, if the corner frequencies in Table 1 were caused by Q, we would find from (2) that

$$Q_\beta/Q_\alpha = t_\beta/t_\alpha \simeq 1.7 \quad . \qquad (3)$$

Most investigators have found that Q_α exceeds Q_β by a factor of 1.5 or more (Takano, 1971; Bakun and Bufe, 1975; Kurita, 1975; Bakun et al., 1975). This discrepancy plus the lack of correlation of R with epicentral distance indicate that Q is not causing the observed corner frequencies.

Lower bounds for Q_β, based on (2), are presented in Table 1. Values are quite high (500-1000) compared with the above-mentioned determinations of crustal Q in western California. The lowest estimate for Q_β in Table 1 (Event 16) is probably not representative, because the event had the shortest travel path (hence lowest value of t in (2)) of the earthquakes studied.

Close-in observations:

Peppin (1975) has presented close-in (a few km) spectra of Event 17, with SV and SH well-defined corner frequencies of 10-12 Hz, above the value given in Table 1. This discrepancy may be a source effect cause by rapid, local sliding on the fault plane (which causes the high close-in corner frequencies) superimposed upon slower sliding over a larger fault segment (which causes the lower corner frequency seen at JAS). Such a mechanism was proposed for the Oroville main shock by Hart et al. (1975).

Coast-Range observations:

Spectral corner frequencies apparently unaffected by propagation would be unusual for such long crustal travel paths. For example, Furuya's (1969) observations are consistent with those of central California earthquakes recorded at Berkeley (more high frequency evident in the P-phase). We have studied the Antioch sequence as recorded at station BRK, 35 km SW, a 3-component broadband system similar to that at JAS. Three events provided excellent spectral data with higher corner frequencies for P than for SV by 40% (Table 1). However, Bakun et al. (1975) report a Q_β of 100 to 150 for a travel path through the Gabilan granites, which represents the most attenuation-free travel path known in west-central California. If we insert $Q_\beta = 150$ in (1), we see that the 3-Hz S-wave corner frequences for these events are very probably caused by attenuation. Then, if $Q_\alpha \geq Q_\beta$, we would see a higher corner frequency for P than for S by (1). Indeed, because of (1) and because generally $Q_\alpha \geq Q_\beta$, we must beware of interpreting corner frequencies in terms of source parameters when the P-wave gives a higher corner frequency than S; such an effect almost always can be explained by attenuation.

Implications for Earthquake Source Theory:

We assume propagation effects have not significantly altered the observed corner frequencies presented in Table 1, so that these corner frequencies measure directly some source parameters. In all recently-published source theories, the dimension of faulting controls the P- and S-wave corner frequencies, and in all but two the predicted variation with azimuth amounts to a factor of 2 or more. Thus, the resolution of the data in Table 1 is adequate to discriminate between source models (subject to the assumption above). Berckhemer and Jacob (1968) employ subsonic rupture propagation velocity, but concentration of energy from the center of a circular dislocation to find equal P- and S-wave corner frequencies. Brune (1970, 1971) and Hanks and Wyss (1972) employ an infinite rupture speed on a circular fault to find higher corner frequencies for P than for S by the ratio of the P- and S-wave velocities. Molnar et al. (1973) use uniform rupture at high propagation velocity on a circular dislocation to find higher values for P- than for S-wave corner frequencies. Sato and Hirasawa (1973) use subsonic rupture propagation on a circular dislocation with greater slip near the center to find higher (> 50%) corner frequencies for P than for S. Burridge (1975) considers self-similar rupture on a circular fault lacking cohesion at the P-wave velocity. His formula (59) for the ratio of the P- to SV-phase corner frequency is 1.2 averaged over the focal sphere, but the ratio is 2 or more on 50% of the focal sphere. Madariaga (1975) solves the problem of slip on a circular crack when stress drop is specified. The slip is concentrated near the center of the crack, and gives slightly higher (10-20%) P-corner frequencies for subsonic rupture propagation. In contrast, Savage (1972) uses a Haskell

fault model with uniform, bilateral, subsonic rupture propagation at 90% of the S-wave speed and uniform fault slip; he finds higher primary corner frequencies for S than for P by a ratio (averaged over the focal sphere) of 1.65 to 1. Similarly, Dahlen (1974) uses a combined dislocation and self-similar crack model at subsonic rupture propagation with uniform fault slip; he finds higher corner frequencies for S than for P (averaged over the focal sphere) by the ratio 2.38 to 1 or 1.75 to 1, depending on whether the rupture propagation velocity is 90% or 80% of the S-wave velocity. In summary, models which have uniform slip and subsonic rupture propagation on circular or bilateral faults predict higher corner frequencies for S than for P at all azimuths, while models which employ supersonic rupture propagation velocity or slip concentrated near the fault center predict higher corner frequencies for P than for S at all azimuths (on the average); Table 2. Of the above-mentioned models, only those of Berckhemer and Jacob (1968) and Madariaga (1975) cannot be excluded by the data of Table 1; but note that the former authors employ what may be an unrealistic assumption, namely rupture propagation velocity decreasing as the faulting front moves out.

The quantity R, then, appears to be a rather sensitive source-model discriminant. Our data could be explained by the models of Berckhemer and Jacob (1968) or Madariaga (1975), but not, for example, by the model of Savage (1972). Bakun et al. (1975) find the opposite: Savage's model can describe their data quite well. None of these three seems capable of explaining the high values of R found by Molnar et al. (1975), but Brune's (1970, 1971) model with a modification by Hanks and Wyss (1972) can. We saw in Table 2 that R depends largely upon the rupture propagation velocity on the fault; it is physically reasonable that this quantity might vary in different source regions (e.g. slower in areas of great heterogeneity, faster on smooth, well-developed fault traces like the San Andreas). That is, we should not be surprised to find that no one model can accurately predict the totality of earthquake phenomena (but

note in Table 2 the features common to the models: each can be formulated as a specific case of Haskell dislocation theory).

The results of this investigation can be explained by another model. If the corner frequency is determined by the time history of motion at the source for these events, then equal and non-varying corner frequencies for P and S would result at all azimuths. This particular model seems physically reasonable for small-to-moderate earthquakes; it implies a source time duration that is long compared with the rupture propagation time acorss the source. This explanation was considered by Johnson and McEvilly (1974) for Central California earthquakes, and would be consistent with the findings of Archuleta and Brune (1975) based on model experiments in foam rubber. More complete azimuthal coverage would be needed to test such a model.

CONCLUSIONS

P- and SV-wave spectral corner frequencies for 18 trans-Sierra earthquakes give a ratio $\underline{R}$ of P-wave to S-wave corner frequency of $.96 \pm .17$. These values appear to be independent of propagation effects, and thus are indicative of conditions at the source of the earthquakes. The SV-wave spectra permit a minimum estimate of Q_β of 480, which is high compared with other California crustal paths previously studied. The precision with which we have determined $\underline{R}$ allows us to eliminate all but two of the recently published source models as applicable to these earthquakes; in this way we find that $\underline{R}$ is a successful discriminant for competing source models.

ACKNOWLEDGMENTS

This research was supported by the Advanced Research Projects Agency of the Department of Defense and was monitored by the Air Force Office of Scientific Research under Grant Nos. F44620-72-C-0069 (University of Nevada) and AFOSR-73-2563 (University of California). Alan Ryall and Tom McEvilly provided criticism that resulted in considerable improvement of the manuscript.

REFERENCES

Archuleta, R. J. and Brune, J. N., Surface strong motion associated with a stick-slip event in a foam rubber model of earthquakes, Bull. Seis. Soc. Am., 65, no. 5, 1059-1072, 1975.

Asada, T. and Takano, K., Attenuation of short period P waves in the mantle, Jour. Physics Earth, 11, #1, 25-34, 1963.

Bakun, W. H. and Bufe, C. B., Shear-wave attenuation along the San Andreas Fault zone in Central California, Bull. Seism. Soc. Am., 65, no. 2, 439-460, 1975.

Bakun, W. H., Bufe, C. B. and R. M. Stewart, Body-wave spectra of Central California earthquakes, Abstracts with Programs, Cordilleran Section 71st Annual Meeting, Geol. Soc. of Am., 7, no. 3, 395, February, 1975.

Berckhemer, H., and K. H. Jacob, Investigation of the dynamical process in earthquake foci by analysing the pulse shape of body waves, Final Sci. Rep. AF61(052)-801, Advanced Research Project Agency Project Vela Uniform, 1968.

Brune, J. N., Tectonic stress and spectra of seismic shear waves from earthquakes, J. Geophys. Res., 75, no. 26, 4997-5009, 1970.

Brune, J. N., Correction, J. Geophys. Res., 76, no. 20, 5002, 1971.

Burridge, R., The effect of sonic rupture velocity on the ratio of S to P corner frequencies, Bull. Seism. Soc. Am., 65, no. 3, 667-676, 1975.

Dahlen, F. A., On the ratio of P-wave to S-wave corner frequencies for shallow earthquake sources, Bull. Seism. Soc. Am., 64, no. 4, 1159-1180, 1974.

Furuya, I., Predominant period and magnitude, J. Phys. Earth, 17, no. 2, 119-126, 1969.

Hanks, T. C. and Wyss, M., The use of body-wave spectra in the determination of seismic source parameters, Bull. Seism. Soc. Am., 62, no. 561-589, 1972.

Hart, R. S., Butler, R., and H. Kanamori, Surface wave and ultra-long period body wave constraints on the August 1, 1975 Oroville earthquake, Trans. Am. Geophys. Union, 57, #12, 1023, 1975.

Kurita, T., Attenuation of shear waves along the San Andreas Fault zone in Central California, Bull. Seism. Soc. Am., 65, no. 1, 277-292, 1975.

Madariaga, R., Dynamics of an expanding circular crack, unpublished manuscript, 1975.

McEvilly, T. V. and Casaday, K. B., The earthquake sequence of September, 1965 near Antioch, California, Bull. Seism. Soc. Am., 57, no. 1, 113-124, 1967.

Molnar, P., Tucker, B. E., and J. N. Brune, Corner frequencies of P and S waves and models of earthquake sources, Bull. Seism. Soc. Am., 63, no. 6, 2091-2104, 1973.

Peppin, W. A., Spectral investigations of the 1 August 1975 Oroville earthquake sequence, Calif. Div. Mines and Geol. Special Report on the Oroville Earthquakes, in press 1975.

Pitt, A. M. and Steeples, D. W., Microearthquakes in the Mono Lake-Northern Owens Valley, California region from September 28 to October 18, 1970, Bull. Seism. Soc. Am., 65, no. 4, 835-844, 1975.

Sato, T. and Hirasawa, T., Body wave spectra from propagating shear cracks, J. Phys. Earth, 21, no. 4, 415-432, 1973.

Savage, J. C., The relation of corner frequency to fault dimensions, J. Geophys. Res., 77, 3788-3795, 1972.

Stump, B. E., P and S wave corner frequencies observed in the near field and the effect of attenuation, E⊕S, Transactions, American Geophys. Union, 56, no. 12, 1148, 1974.

Takano, K., A note on the attenuation of short period P and S waves in the mantle, J. Phys. Earth, 19, no. 2, 155-163, 1971.

TABLE 1

Event no.	Date-Time	Location	ΔJAS (km)	M_L (4)	f_cP (5) (Hz)	f_cS (5) (Hz)	R	$Q_\beta \geq$ (7)
1	06 July 1974 061040	38.77 N 119.63 W	114	3.7	3.8 (G)	5.0 (E)	.76	710
2	13 Aug 1974 144420	38.69 N 119.10 W	137	3.3	2.8 (F)	2.9 (E)	.97	495
3	14 Nov 1974 162039	37.77 N 118.30 W	174	3.3	2.9 (G)	2.8 (G)	1.04	610
4	18 Nov 1974 020453	37.72 N 118.72 W	160	3.2	4.8 (G)	4.3 (G)	1.12	860
5	21 Nov 1974 125523	37.77 N 118.25 W	180	3.4	2.1 (P)	2.3 (G)	.91	515
6	07 Dec 1974 021830	37.99 N 118.79 W	149	3.3	3.0 (G)	3.2 (E)	.94	595
7	25 Feb 1975 111322	37.1 N 117.9 W (1)	251	4.0	2.7 (G)	2.7 (G)	1.00	845
8	05 May 1975 062954	38.61 N 119.73 W	97	3.6	4.3 (G)	3.9 (E)	1.10	(470)
9	05 May 1975 065152	38.61 N 119.73 W	97	3.2	4.0 (G)	4.7 (G)	.85	570
10	07 May 1975 093543	38.61 N 119.73 W	97	3.6	3.7 (F)	3.5 (E)	1.06	(425)
11	01 Aug 1975 212924	39.45 N 121.55 W (2)	175	3.6	3.0 (F)	3.1 (G)	.97	680
12	02 Aug 1975 005248	39.48 N 121.51 W (2)	175	3.8	2.4 (P)	2.5 (G)	.96	545
13	02 Aug 1075 105151	39.47 N 121.49 W (2)	175	3.7	1.5 (P)	2.1 (G)	.71	460
14	04 Aug 1975 094745	39.42 N 121.52 W (2)	175	3.5	2.3 (G)	2.8 (F)	.82	610
15	06 Aug 1975 164152	39.50 N 121.53 W (2)	175	3.6	2.0 (G)	1.4 (G)	1.42	305
16	10 Aug 1975 151640	37.37 N 119.99 W (2)	77	3.8	2.3 (G)	3.0 (E)	.77	(290)
17	16 Aug 1975 054809	39.47 N 121.52 W (2)	175	4.0	2.5 (F)	2.2 (G)	1.14	480
18	17 Aug 1975 002426	37.53 N 120.40 W (2)	160	3.7	2.7 (F)	3.4 (G)	.79	680
A	10 Sept 1965 213811	38.00 N 121.83 W (3)	35 (6)	2.6	4.0 (G)	3.2 (G)	1.25	140
B	11 Sept 1965 000833	38.00 N 121.85 W (3)	35 (6)	2.8	4.0 (F)	3.1 (G)	1.29	135
C	11 Sept 1965 001540	38.01 N 121.85 W (3)	35 (6)	2.4	4.8 (G)	3.2 (F)	1.5	140

TABLE 1 nt.)

(1) PDE location

(2) Berkeley locations

(3) McEvilly and Casaday (1967)

(4) Berkeley Wood-Anderson magnitudes

(5) reproducability of measurements (estimate)

E: 5%
G: 10%
F: >10%
P: not well-defined

(6) distance to Berkeley

(7) estimate presumed low if included in parentheses

TABLE 2. Essentials of Recent Source Theories

Author	Fault Shape	Rupture Propagation Velocity	Direction of Fault Rupture	Nature of Slip	Predicted R	Reference
Berckhemer and Jacob (1968)	circular	subsonic, variable	radial	uniform	near 1	Savage (1972) p. 3792
Brune (1970, 1971)	circular	instantaneous	simultaneous	uniform	1.7	Brune (1971)
Hanks and Wyss (1972)	circular	instantaneous	simultaneous	uniform		equation (7)
Molnar et. al. (1973)	circular	supersonic	radial out, then radial in	uniform or concentrated near center	1.7	p. 2099
Sato and Hirasawa (1973)	circular	subsonic	radial	concentrated near center	>1.5	Table 2
Burridge (1975)	circular	supersonic	radial	uniform	1.25-1.5	equation (59)
Madariaga	circular	subsonic	radial	concentrated near center	1.0-1.2	Figure 10
Savage (1972)	rectangular	subsonic	bilateral	uniform	.61	equation (13)
Dahlen (1974)	circular or elliptical	subsonic	radial	uniform	.42-.57	equation (41)

THE OROVILLE EARTHQUAKE SEQUENCE OF AUGUST 1975 *

Paul W. Morrison, Jr.

Earthquake Engineering
Department of Water Resources
P.O. Box 388
Sacramento, California
95802

Brian W. Stump and Robert Uhrhammer

Seismographic Station
Department of Geology and Geophysics
University of California, Berkeley
Berkeley, California
94720

ABSTRACT

The characteristics of the Oroville, California earthquake sequence of 1975 are presented. Historically, the Oroville area is one of low seismicity; the largest earthquake in the region occurred with a magnitude 5.7 in 1940 some 50 km north of Oroville. This low seismicity continued through initial loading of nearby Oroville Dam in 1967-68 and until the first foreshock on June 28, 1975. Twenty-one foreshocks ($M_L \geq 1.6$), the largest of magnitude 4.7, preceded the magnitude 5.7 main shock of 01 August. All foreshocks and aftershocks of $M_L \geq 3.0$ were located using seismographs operated by the University of California at Berkeley, USGS, and the California Department of Water Resources. The aftershock region covers an area approximately 14 km by 10 km southeast of the city of Oroville. The depth distribution of the earthquakes indicates a west dipping fault plane. The b value of 0.61 shows the sequence to be rich in larger magnitude aftershocks. Similar b values have been determined for other aftershock sequences in California, such as a sequence near Coalinga in August 1975. The aftershock occurrence rate follows an Omori relation with $n(t) \propto t^{-.70}$. Apparent variability in the earthquake mechanisms of the series makes interpretation of composite fault plane solutions difficult, but the data indicate normal faulting striking NNW and a west dip of about 30° - 40°, the Sierra Nevada moving up with respect to the Great Valley.

* In press, Bull. Seism. Soc Amer., Aug., 1976.

SUMMARY VERSION OF PAPER IN PRESS

On August 1, 1975 at 2020 GMT(1320 PDT) a magnitude 5.7 earthquake occurred 12 kilometers southwest of Oroville Dam (Figure 1) and caused some damage in the city of Oroville and vicinity. This earthquake was preceded by foreshocks beginning on June 28, 1975, the largest of which had M_L = 3.5 (Table 1); the sequence appeared to have died out (only five events between July 8 and August 1), when on August 1, 11 foreshocks with magnitude less than 4.8 occurred within five hours of the main shock.

The results of seismic monitoring near Oroville are shown in Figure 2. The histogram shows numbers of earthquakes within 10 kilometer increments of radius out to 50 kilometers from ORV. The increase in seismicity in Figure 2 from 1968 to 1975 reflects the 5-6 fold increase in magnification achieved with the switch from paper (U. C. Berkeley) to 16 mm film (DWR) records.

The elevation of the water surface of Lake Oroville is also shown in Figure 2. From November 1967 until March 1968, the reservoir filled to half its capacity (water surface elevation 229 m). The reservoir was first filled to capacity in July 1969. The largest annual level fluctuations occurred in the winter of 1974-75 when the reservoir level reached a low of 230 m elevation. This draw-down is equivalent to 48% of the reservoir capacity. In prior years the draw-down was typically about 25%. During the seven year period of large water storage, the histogram indicates no significant fluctuations in the local seismicity near to the dam (< 30 km). The very low level of local activity continued through the 1974-75 rapid draw down and recharge.

On June 28, the foreshocks of the 1975 Oroville series began. These events are shown on the histogram of Figure 2 in the 0-10 and 10-20 km ranges. As a reaction to the earthquake of June 28, the portable seismograph stations Butte City (BUT) and Sutter Butte (SUT) were established on July 1, 1975. Locations are shown in Figure 3.

The magnitude of the mainshock is estimated to be 5.7 on the Richter scale. This value was obtained by averaging the individual estimates from Wood-Anderson seismographs at Arcata, 5.7; Berkeley, 5.7; Stanford, 5.7 (T. Hanks personal communication); and Mount Hamilton, 5.6 (one component). No estimate was obtained from the instrument at Mineral as its recordings were off-scale.

The hypocentral parameters and Richter magnitudes of the 51 earthquakes ($M_L \geq 3.0$) of the Oroville sequence occurring between June 28 and August 16, 1975 are listed in Table 1. Locations of these earthquakes are shown in Figure 4. The bars in the figure represent standard errors. The aftershock region covers an area approximately 10 km by 14 km centered 8 km southeast of Oroville. The earthquakes are generally deeper in the western part of the aftershock zone, with depths ranging from 1.5 to 9.2 km.

The Oroville sequence through August 11 consisted of 21 foreshocks, the main shock, and 292 aftershocks with Richter magnitude of 1.6 or above. Twelve aftershocks with $M_L \geq 4.0$ were recorded during the same time period. A graphical representation of the earthquake sequence is shown in Figure 5.

The frequency of occurrence shown in Figure 6 may be fitted to Omori's relation: $n(t) = A/(t+C)^p$. Aftershocks were divided into cells, each containing 15 earthquakes, and the average occurrence time plotted for each cell. The least squares solution gave $p = 0.70$.

Magnitude occurrence data are summarized in Figure 7 where N represents the cumulative number of earthquakes of magnitude greater than or equal to M_L. The M_L values are plotted in magnitude increments of one tenth. The equation $\log N = a - bM_L$ was fitted by least-squares and yielded $b = 0.61$. The main event magnitude is included in the solution. The b value changes by less than 2% if the main event is removed or if only events of $M_L \geq 2.8$ are used.

Composite fault plane solutions were determined for earthquakes in the northern, west central, and southern parts of the aftershock zone. Due to the limited data, well-resolved fault planes were difficult to obtain. The northern and west central parts of the aftershock zone clearly indicate normal faulting with the mountains to the east up with respect to the valley to the west. The group of 4 earthquakes to the north (Figure 8a) yields a solution with a strike of between N 10° W to N 20° E and a west dip of approximately 40°. The west central section (Figure 8b) indicates a fault strike range of N 10° W to N 30° W with a west dip of 30°. No coherent solution could be found for the southern group.

Testing JAS and WDC broadband systems for large motions:

The Oroville shock provided an excellent test of the broadband flat displacement channels at JAS (195.5 km, 151.3° Az) and WDC (149.6 km, 324.4° Az). Figures 8 and 9 show magnetic tape playouts from the stations. High- and low-gain displacement channels differ in gain by 200, as indicated.

The low-gain channels behaved very well, recording nearly 2 mm of ground displacement with no indication of spurious seismometer response such as spring resonance or impulsive responses to zero position shifts frequently seen in long period systems.

The high-gain displacement channels also behaved well. Interestingly, the long period (10-20 sec) motion generated by this shock was visible on these records for several hours, possibly reflecting surface wave energy trapped and resonating within the Great Valley.

In conjunction with excellent data obtained at short distances by local networks, the regional broadband recordings will provide excellent information on this earthquake.

References

Bolt, B.A. and B.S. Gopalakrishnan (1975). Magnitudes, Aftershocks, and Fault Dynamics; San Fernando California Earthquake of 9 February 1971; California Division of Mines and Geology Bulletin 196, Chapter 21.

Bolt, B.A., C. Lomnitz, and T.V. McEvilly (1968). Seismological Evidence on the Tectonics of Central and Northern California and the Mendocino Escarpment, Bull. Seism. Soc. Am., 58, 1725-1767.

Bolt, B.A. and R.D. Miller (1971). Seismicity of Northern and Central California, 1965-1969, Bull. Seism. Soc. Am., 61 (6), 1831-1847.

Comninakis, P., J. Drakopoulos, G. Moumanlidis, B. Papazachos (1968). Foreshock and Aftershock Sequences of the Kremasta Earthquake and Their Relation to the Waterloading of the Kremasta Artificial Lake, Ann. Geofis., 21 (1), 39-71.

Earthquakes in Kern County, California During 1952, California Division of Mines Bulletin 171, 1955.

Galanopoulos, A.G. (1967). The Influence of the Fluctuation of Marathon Lake Elevation on Local Earthquake Activity in the Attica Basin Area (in Greek), Ann. Geol. Pays Hellen., 18, 281-306.

Gough, D.I. and W.I. Gough (1970a). Stress and Deflection in the Lithosphere Near Lake Kariba, 1, Geophys. J. Roy. astro. Soc., 21, 65-78.

Gough, D.I. and W.I. Gough (1970b). Load Induced Earthquakes at Lake Kariba, 2, Geophys. J. Roy. astro. Soc., 21, 79-101.

Gupta, H.K., B.K. Rastogi, and H. Narain (1972b). Some Discriminatory Characteristics of Earthquakes Near the Kariba, Kremasta, and Koyna Artificial Lakes, Bull. Seism. Soc. Am., 62, 493-507.

Gupta, H.K., B. K. Rastogi, and H. Narain (1973). Earthquakes in the Koyna Region and Common Features of the Reservoir-Associated Seismicity, Man-Made Lakes: Their Problems and Environmental Effects: American Geophysical Union, Washington, D.C., 455-467.

McEvilly, T.V., W. H. Bakun, and K.B. Cassady (1967). The Parkfield, California, Earthquakes of 1966, Bull. Seism. Soc. Am., 57, 1221-1244.

Scholz, C. (1971). Microearthquakes on the San Andreas Fault and Aftershocks of the San Fernando Earthquake, The San Fernando, California Earthquake of February 9, 1971, U.S. Department of Interior - U.S. Department of Commerce, U.S. Government Printing Office, Washington, 33-37.

Utsu, T. (1961). A Statistical Study on Occurrence of Aftershocks, The Geophysical Magazine, 3(4), 521-616.

Acknowledgments

Data for this study were generously supplied by several individuals and groups. We are particularly grateful to Woody Savage (Woodward Clyde Consultants), Charles Bufe (USGS), and Dave Kessler (DWR). Professors Bruce Bolt and Thomas McEvilly offered valuable suggestions and criticism.

Funds for this study were provided in part from National Science Foundation Grant Number AEN 74-21548 and Air Force Office of Scientific Research Grant Number 73-2563.

TABLE 1: Earthquake data for events with $M_L \geq 3.0$.

	Date	Origin Time (OT)	σ(T)sec	Magnitude M_L	Latitude φ	σ(φ)km	Longitude λ	σ(λ)km	Depth h	σ(h)km
1	28 JUN 75	041953.72	0.13	3.5	39°28.33'	1.19	121°31.45'	1.05	7.56km	1.59
2	01 AUG 75	154537.81	0.07	3.8	39 26.98	0.67	121 31.87	0.67	7.27	1.06
3	01 AUG 75	162717.81	0.14	4.7	39 26.29	1.19	121 32.25	1.20	4.89	2.17
4	01 AUG 75	172650.12	0.09	3.0	39 27.71	0.85	121 32.27	0.83	8.57	1.22
5	01 AUG 75	202004.75	0.08	4.5	39 26.33	0.76	121 31.71	0.76	8.01	1.17
6	01 AUG 75	202012.85		5.7	39 26.33		121 31.71			
7	01 AUG 75	2025		4.7	39 26.33		121 31.71			
8	01 AUG 75	2029		4.6	39 26.33		121 31.71			
9	01 AUG 75	203239.84	0.15	3.0	39 26.71	1.62	121 30.40	1.44	4.82	3.21
10	01 AUG 75	2037		3.5	39 26.71		121 30.40			
11	01 AUG 75	2045		3.0	39 26.71		121 30.40			
12	01 AUG 75	204618.40	0.14	3.8	39 28.40	1.56	121 30.02	1.59	6.13	2.69
13	01 AUG 75	210539.84	0.04	3.0	39 25.98	0.38	121 29.25	0.43	6.74	0.63
14	01 AUG 75	212150.65	0.07	4.1	39 26.53	0.64	121 31.70	0.64	7.76	0.99
15	01 AUG 75	212559.02	0.04	3.3	39 28.44	0.42	121 31.08	0.41	7.08	0.63
16	01 AUG 75	212924.12	0.08	3.6	39 27.12	0.69	121 32.92	0.80	6.55	1.21
17	01 AUG 75	234440.98	0.03	3.4	39 29.18	0.25	121 31.34	0.24	7.51	0.35
18	02 AUG 75	005248.47	0.03	3.8	39 29.06	0.25	121 30.55	0.24	7.27	0.36
19	02 AUG 75	063157.19	0.06	3.2	39 26.84	0.50	121 29.01	0.38	5.68	0.79
20	02 AUG 75	101153.68	0.04	3.1	39 29.40	0.37	121 30.70	0.35	7.22	0.52
21	02 AUG 75	104900.12	0.07	3.3	39 25.66	0.52	121 28.41	0.43	5.54	0.85
22	02 AUG 75	115150.74	0.12	3.4	39 28.36	0.89	121 29.30	0.91	2.49	1.86
23	02 AUG 75	144438.71	0.04	3.2	39 25.03	0.32	121 29.38	0.33	5.00	0.59
24	02 AUG 75	165145.11	0.05	3.7	39 25.07	0.43	121 29.09	0.44	6.48	0.75
25	02 AUG 75	172429.23	0.07	4.3	39 28.42	0.60	121 28.25	0.59	5.84	0.98
26	02 AUG 75	174324.13	0.06	4.0	39 28.66	0.51	121 28.41	0.49	5.52	0.83
27	02 AUG 75	195836.85	0.05	3.1	39 26.89	0.44	121 32.20	0.44	7.10	0.70
28	02 AUG 75	202216.32	0.05	5.1	39 26.69	0.35	121 27.76	0.36	3.62	0.71
29	02 AUG 75	203548.55	0.06	3.9	39 28.26	0.52	121 28.89	0.51	5.98	0.84
30	02 AUG 75	205855.70	0.06	3.8	39 25.93	0.50	121 27.97	0.51	5.71	0.90
31	02 AUG 75	2059		5.2	39 25.93		121 27.97			
32	02 AUG 75	214001.34	0.07	3.9	39 25.62	0.57	121 28.39	0.58	5.39	1.04

TABLE 1 (Continued)

33	03 AUG 75	010305.77	0.04	4.6	39 29.26	0.40	121 31.06	0.38	7.98	0.55
34	03 AUG 75	024708.80	0.04	4.1	39 28.68	0.33	121 30.06	0.32	6.79	0.50
35	04 AUG 75	094745.01	0.06	3.5	39 25.27	0.61	121 31.36	0.45	7.57	0.88
36	05 AUG 75	022857.35	0.05	3.3	39 24.91	0.39	121 29.46	0.33	7.17	0.63
37	05 AUG 75	204424.50	0.17	3.2	39 24.87	1.35	121 30.87	1.15	6.79	2.23
38	06 AUG 75	035029.94	0.20	4.7	39 28.73	1.94	121 31.46	1.73	7.69	2.51
39	06 AUG 75	162547.93	0.14	3.1	39 26.73	1.24	121 27.58	1.14	8.49	1.30
40	06 AUG 75	164152.08	0.02	3.6	39 29.80	0.17	121 31.76	0.17	8.40	0.16
41	06 AUG 75	210033.46	0.11	3.0	39 26.37	0.95	121 29.10	0.89	9.20	0.98
42	06 AUG 75	2100		3.0	39 26.37		121 29.10			
43	07 AUG 75	203120.38	0.15	3.1	39 30.99	1.56	121 31.98	1.48	8.68	1.71
44	08 AUG 75	070050.09	0.05	4.9	39 30.13	0.51	121 30.72	0.46	7.64	0.62
45	08 AUG 75	133753.87	0.08	3.2	39 29.79	0.70	121 29.37	0.64	6.29	0.68
46	08 AUG 75	190327.23	0.09	3.1	39 23.60	0.65	121 29.60	0.62	5.60	0.91
47	09 AUG 75	073847.48	0.10	3.0	39 24.80	0.74	121 29.00	0.70	7.46	0.90
48	11 AUG 75	024016.73	0.35	3.0	39 27.72	2.28	121 26.53	1.85	1.52	3.89
49	11 AUG 75	061136.34	0.12	4.3	39 26.78	0.91	121 28.85	0.81	4.26	1.24
50	11 AUG 75	155905.26	0.19	3.6	39 28.22	1.40	121 33.23	1.39	6.39	1.68
51	16 AUG 75	054809.38	0.03	4.0	39 28.33	0.33	121 31.26	0.40	9.01	0.51

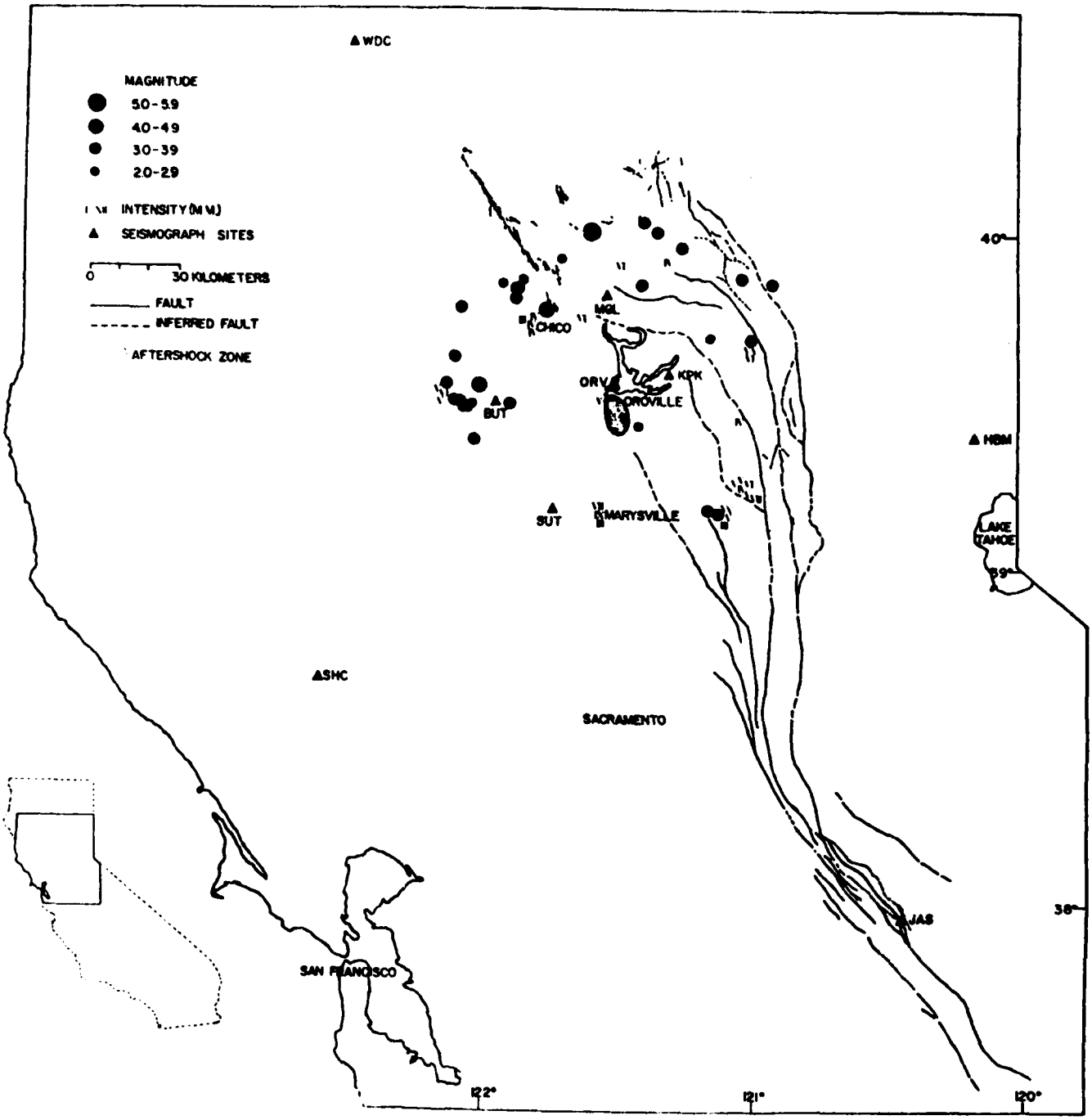

FIGURE 1: Station locations and historical seismicity within 60 km of Oroville.

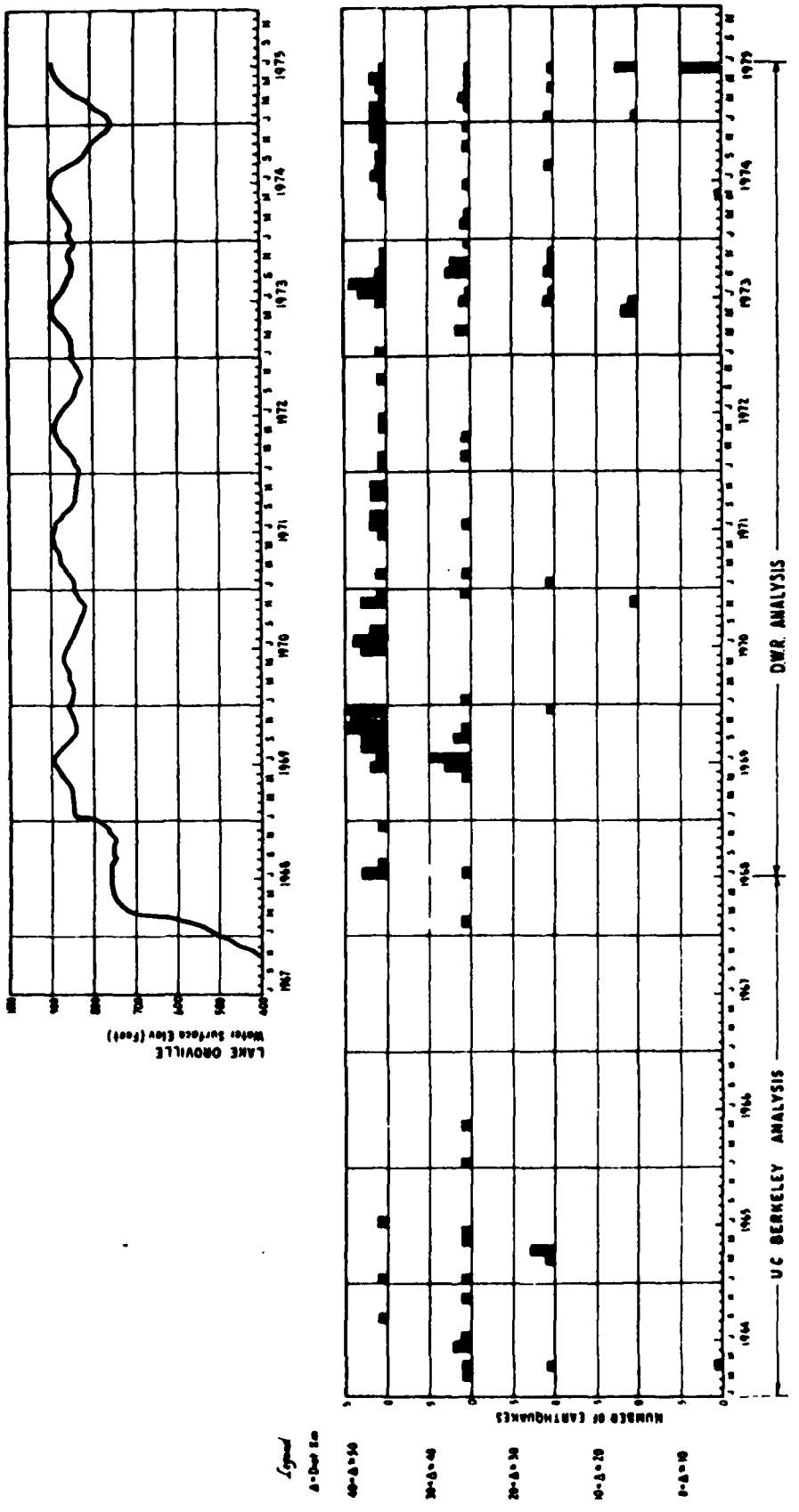

FIGURE 2: Local earthquakes in the Oroville area and Lake Oroville water surface elevation.

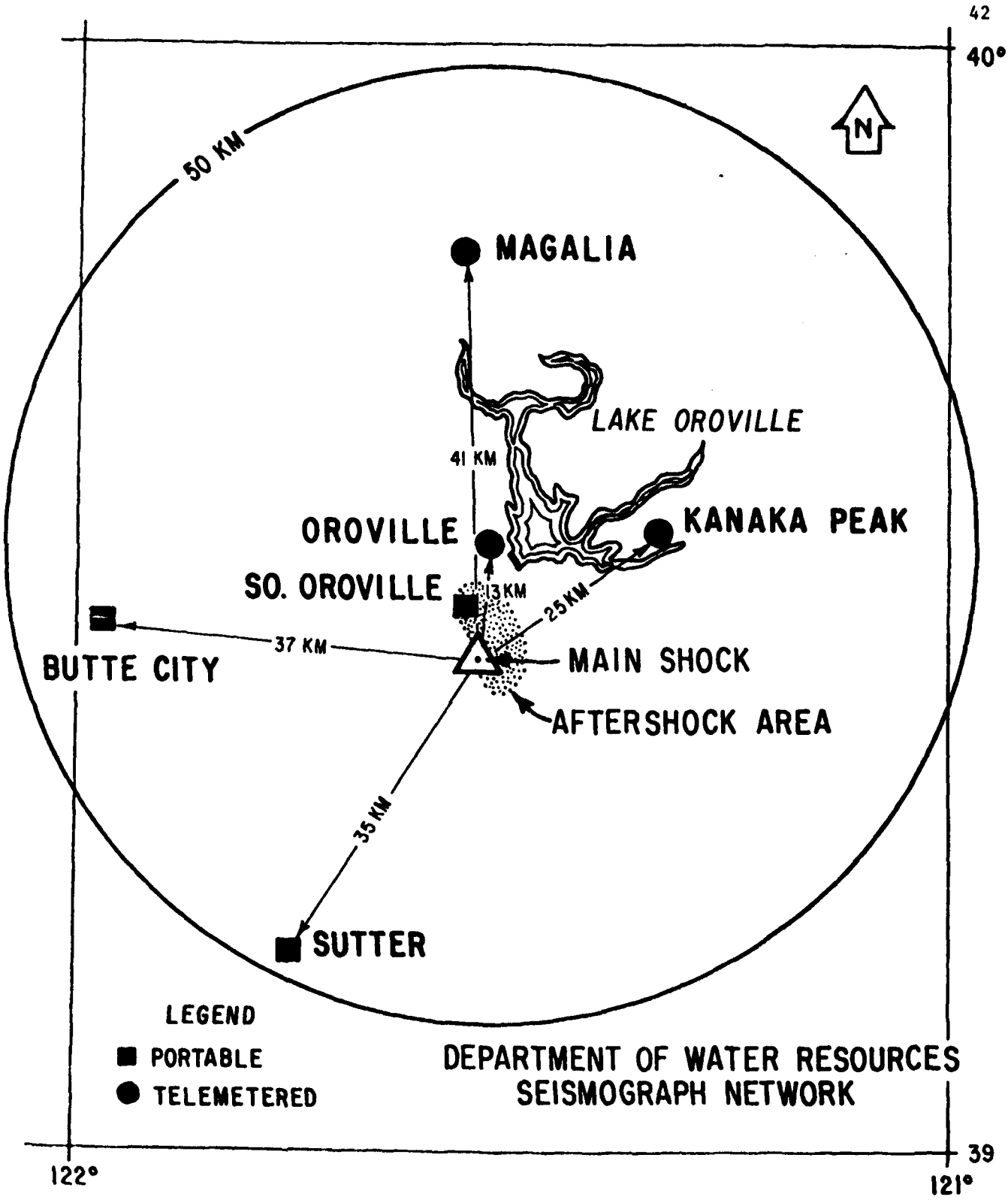

FIGURE 3: Department of Water Resources local seismographic network.

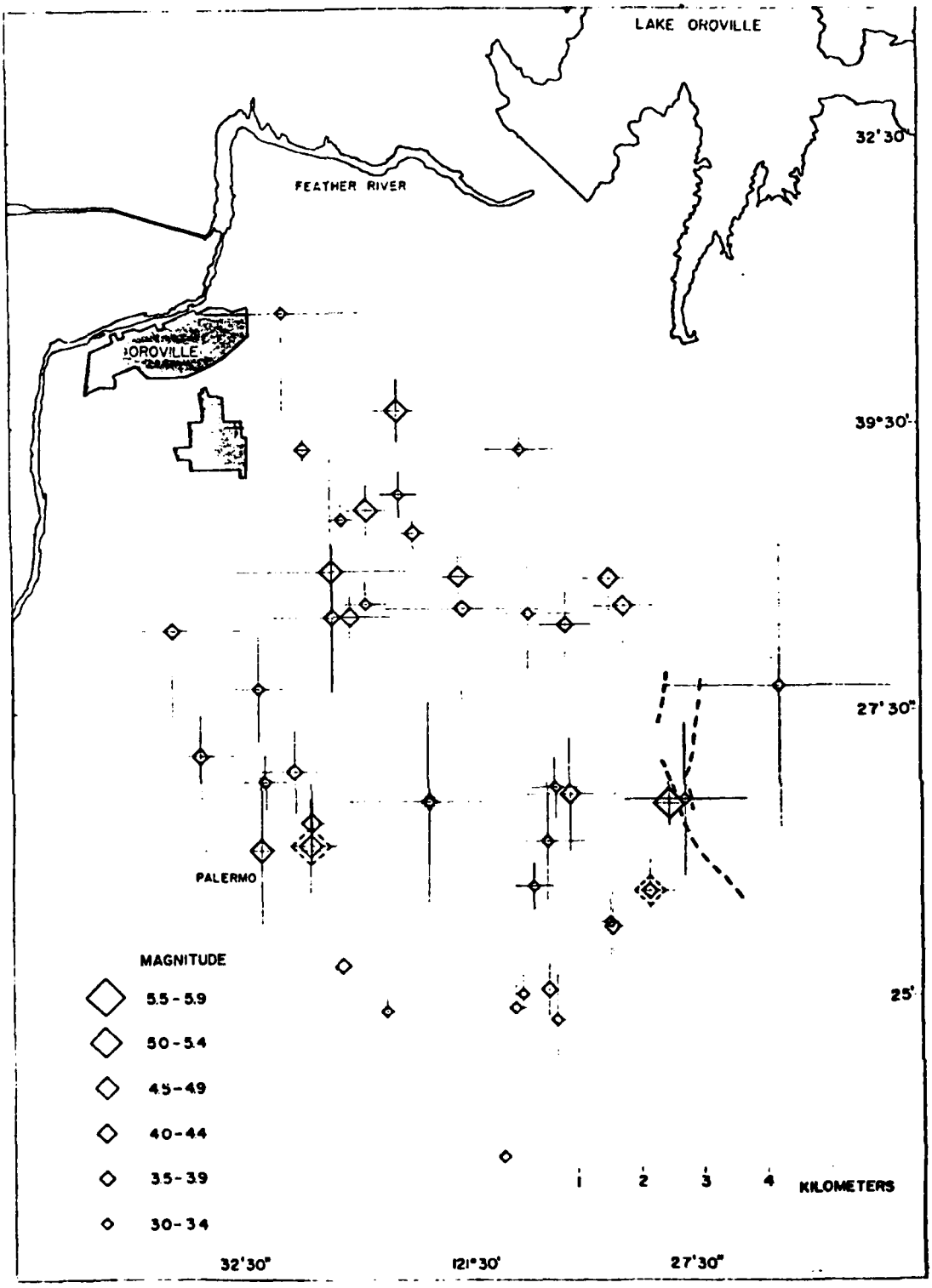

FIGURE 4: Earthquake locations of the Oroville sequence. Standard errors in location estimated by least squares are indicated by bars through the epicenters. Dashed diamonds represent earthquakes whose locations are assumed to be those of their immediate foreshocks. The dashed lines indicate the lines of surface cracks observed after the main shock.

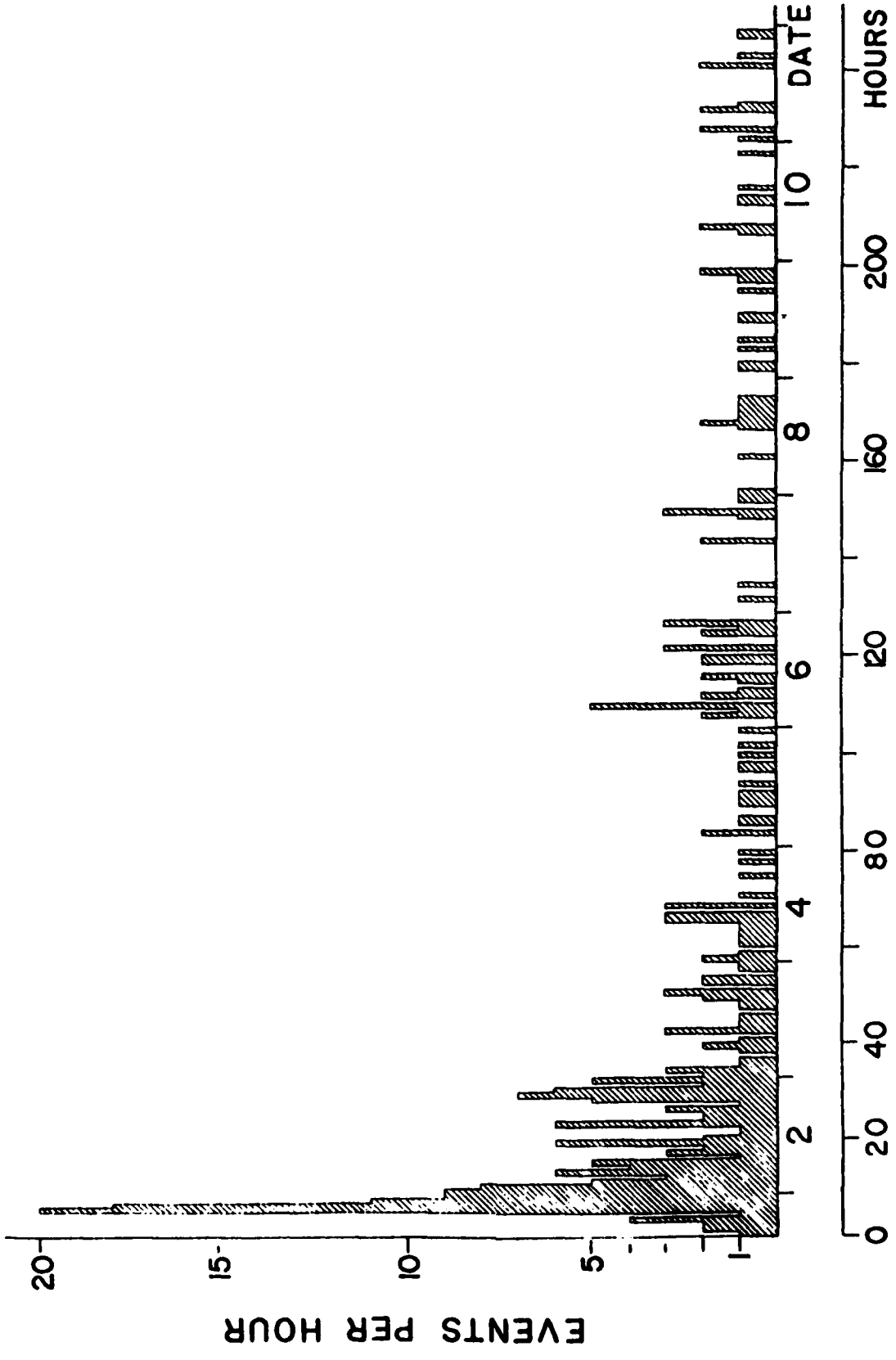

FIGURE 5: Frequency of occurrence of the earthquakes in the Oroville sequence from 1500 (GM 01 August to 0000 (GMT) 12 August.

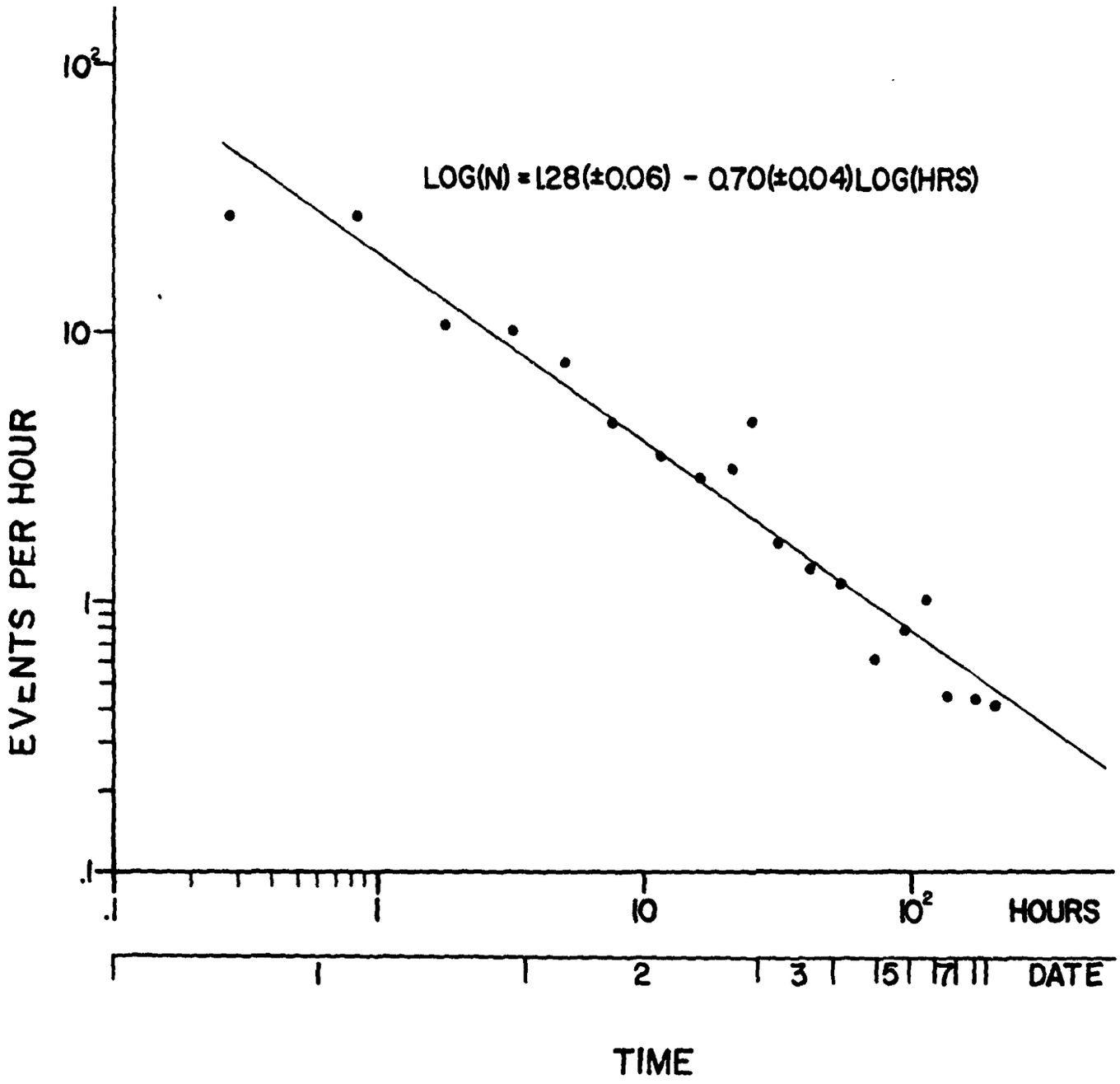

FIGURE 6: Logarithmic representation of Figure 5 fitting an Omori type law $n(t) \propto t^{-.70}$.

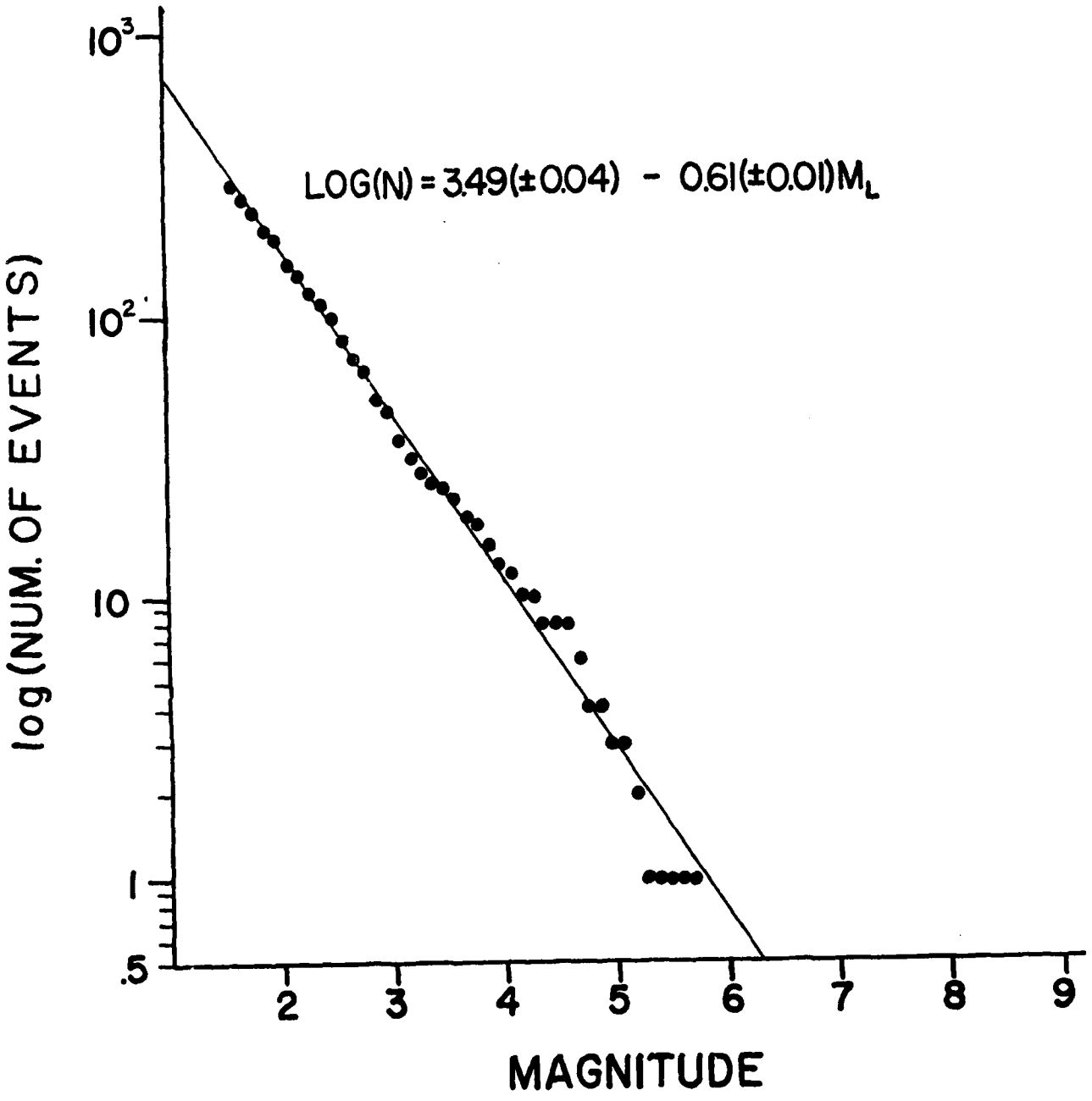

FIGURE 7: Plot of log N vs M_L ($M_L \geq 1.6$). The solid line is the least squares fit to the data.

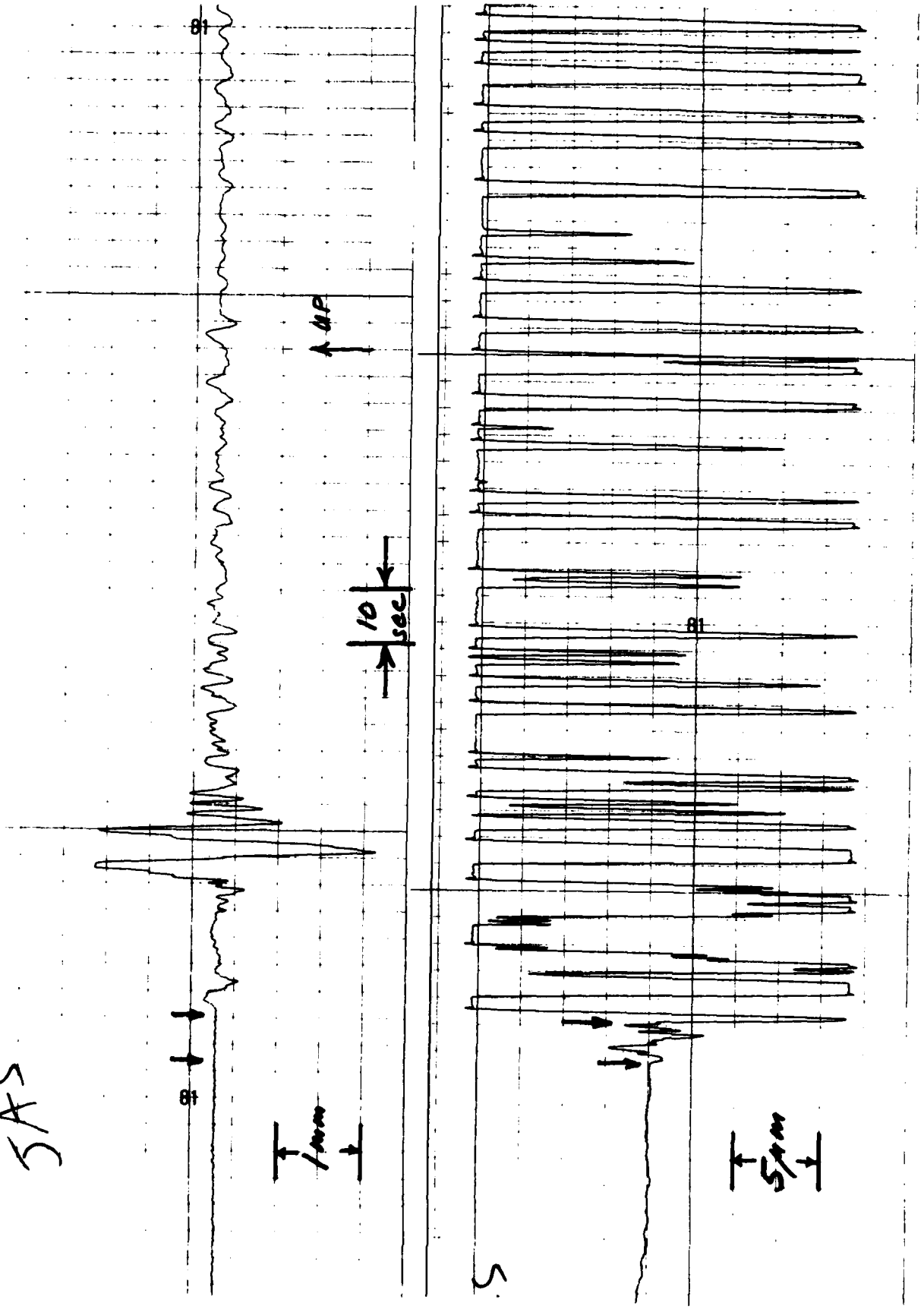

Figure 8. Broadband recordings of the 01Aug75 Oroville earthquake at JAS, vertical component. Low-gain (upper) channel is ±2mm full scale ground motion; high-gain channel is ±10microns full scale. Arrows indicate P-wave arrivals for foreshock and main shock.

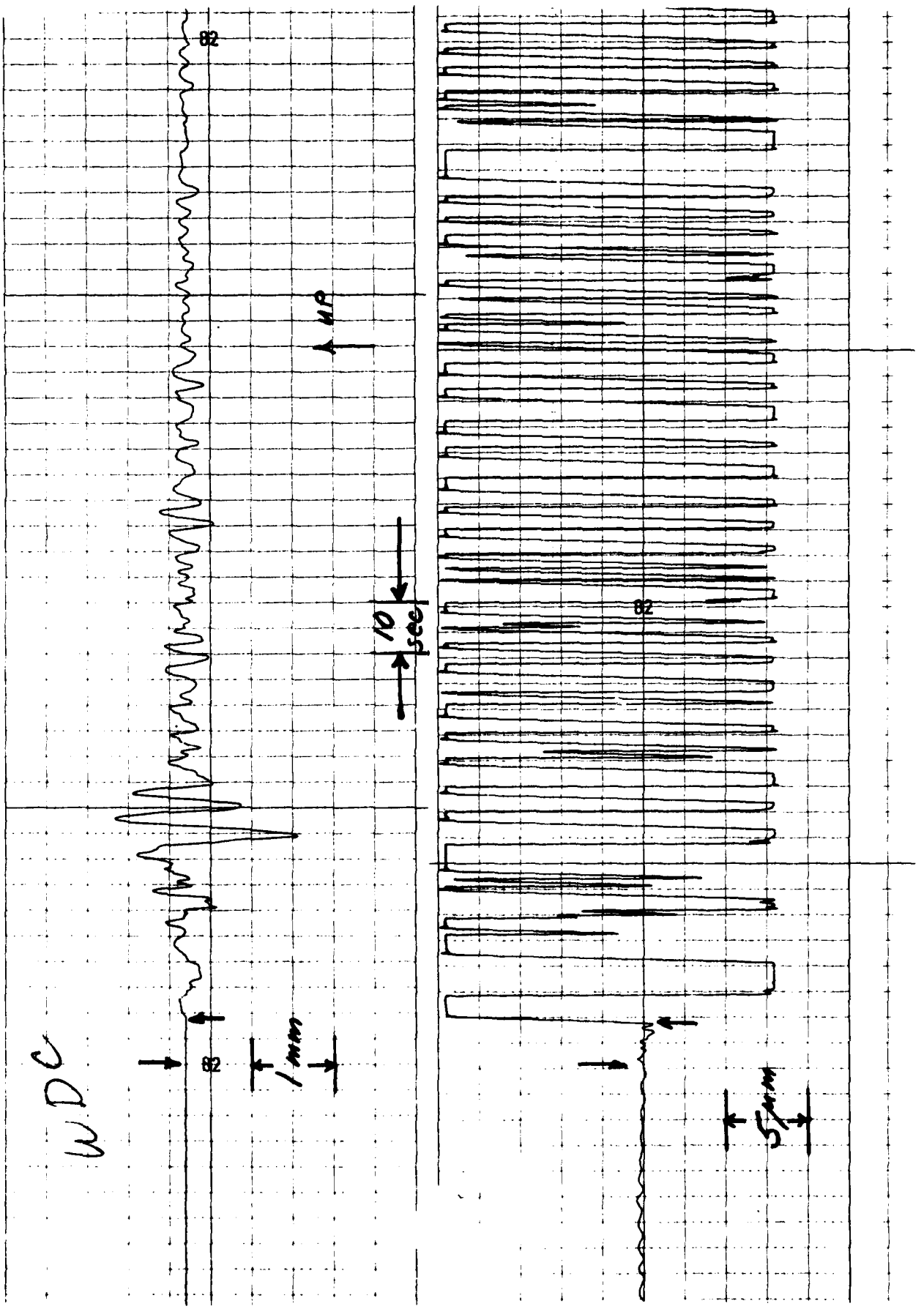

Figure 9. Same as Figure 8 but for WDC.